The University of Cambridge

Part III essay

Wound Healing Angiogenesis

Author:
Tom Bury

Supervisor:
Dr. Julia Gog

Contents

Chapter 1

Introduction

1.1 Motivation for study

Over the course of evolution, mammals have developed complex mechanisms for the control and recovery of wounds. Angiogenesis, the formation of blood vessels from pre-existing vasculature, is the crucial component to this process. Within angiogenesis, there are many chemical processes involved, and hence a large range of biologically-plausible parameters. Many models have been proposed, adopting various approaches. In this review we will explore these models and take a look at their relative strengths and weaknesses, noting why they were proposed and what benefit they have had to the understanding of angiogenesis.

Why might one wish to model angiogenesis mathematically? Not only is it involved in wound healing, angiogenesis occurs during embryogenesis, arthritis and during the growth of solid tumours. The primary motivation for this work lies in the scope of developing practical clinical treatments for both mediating wound angiogenesis and for inhibiting tumour angiogenesis (solid tumours cannot become malignant without it). The models allow us to investigate the qualitative nature of angiogenic response and identify the most important mechanisms involved. With the parameter values for the models having been based on experimental data, the model simulations give close comparisons to the reality of the process.

1.2 The Process of Angiogenesis - a biological description

As previously noted, angiogenesis occurs during many mammalian growth processes, some of which we wish to speed up (wound healing etc.), others we wish to control (as with tumour growth). In each case however, the well-ordered sequence of events characterising angiogenesis is the same.

The first notable event is the degradation of the basement membrane of the capillary cells near to the wound site. The basement membrane consists of laminae which coat the exterior of the blood capillaries. Its role is to maintain endothelial stability, impermeability, and resistance against

hydrostatic pressure. The degradation allows endothelial cells from within the capillary to migrate out through the ruptured membrane and toward the wound site.

At vessel locations where the membrane is ruptured, the endothelial cells adopt a migratory and proliferative phenotype. Those which migrate out form a sprout tip which extends from the parent vessel, mediated by the extracellular matrix (ECM). Further sprout extension occurs when some of the endothelial cells just behind the sprout tip proliferate. Given a high enough cell density, sprouts can split and move off in separate directions. This is known as sprout branching and is key in forming a strong dendritic capillary structure on the wound bed.

Initially, the sprouts grow out from the parent vessel approximately parallel to each other. After a certain distance, branches of the sprouts tend to incline toward each other and can fuse together to form a loop through which blood can flow. This process is known as anastomosis. Following this, new sprouts can emerge repeating the angiogenic sequence to provide further extension to the new capillary bed. This continues until the wound site is permeated by a full network of capillaries.

In some cases, the natural angiogenic response is not enough for a full wound recovery. Indeed, for severe wounds or angiogenic systems that are lacking in certain chemicals, intervention is required to aid the recovery process. Models of unsuccessful healing and possible treatments will be investigated in Chapter 5.

Chapter 2

Considerations when Constructing a Model

Upon translating proposed biological models to mathematical form, systems that arise tend to take the form of coupled reaction-diffusion equations. Our mathematical framework will be based on the conservation equations for the concentrations c_i (i=1...9) of the n substances we are modelling. These are given by

$$\frac{\partial c_i}{\partial t} + \nabla.\vec{J_i} = f_i \quad \text{for i=1...n} \tag{2.1}$$

where the J_i are fluxes and the f_i are the local kinetics which in general can both depend on the c_j for j=1...n. This couples the equations together through interaction terms.

Within this system of equations, there are many important factors we need to take into account in building a framework for angiogenesis. The following sections point out what needs be considered and gives examples of what has already been trialled in the literature.

2.1 Inter-dependent Variables

The interacting diffusion equations can be solved numerically to examine the distribution in space and time of the variables we chose to include. Depending on the governing chemical processes and kinetics, each variable provides a unique contribution to the overall dynamics of the system.

The process of angiogenesis is complex, involving a large number of variables that interact in various ways, making it challenging to model mathematically. An ideal model strikes a balance between keeping the number of variables down, thereby making the model as simple as possible, while at the same time including a sufficient number so as not to exclude any important phenomenon. We shall view both sides of the spectrum, and the relative merits to each approach.

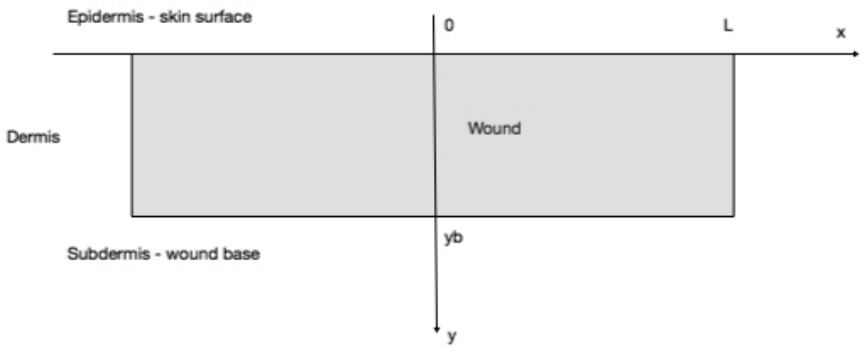

FIGURE 2.1: Cross section of the dermal wound model

The most involved model we consider [1] uses six variables, which are considered to be of the greatest importance in angiogenesis. They include densities of capillary tips, capillary sprouts, endothelial cells, fibroblasts, chemoattractants, oxygen and extracellular matrix. Other models [2–4] work with a minimalist approach, involving only the two model constituents which best represent a certain feature of angiogenesis. Both approaches produce interesting results which agree to a large extent with experimental observation.

2.2 Number of Spatial Dimensions

In this review, we will limit ourselves to incisional wounds, which reduces the problem to one on a two dimensional domain, representing the vertical plane of the wound. This is shown in Figure 2.1. Initially, we shall neglect the effects of wound depth and work simply in one dimension where $-L \leq x \leq L$ defines the wound space, the wound centre at $x = 0$. In practise however, a significant component of dermal healing proceeds from the base of the wound toward the upper surface. Olsen et al. [3] analyse two dimensional simulations of a model encapsulating the cell-ECM interactions that take place during angiogenesis. This will be investigated in Chapter 4.

In Chapter 6 we introduce a model for tumour-induced angiogenesis. In this case, working with multiple dimensions is essential in order to capture the formation of the capillary structure. A three dimensional model is proposed in Chapter 7 for the approach of endothelial cells towards a spherical source of tumour cells.

2.3 Initial and Boundary Conditions

We are going to assume the wound takes the form of a slit (two dimensional) with reflectional symmetry about its centre-line perpendicular to the skin. Thus we only need consider the semi-infinite domain $x \geq 0$, $0 \leq y \leq y_b$ where y_b defines the depth of the wound. This is illustrated in Figure 2.1.

In order to find a particular solution to the interacting diffusion equations, we require initial and boundary conditions, as outlined below.

By the requirement of symmetry, there must be zero horizontal flux at $x = 0$ for all time giving a Neumann boundary condition (fluxes will be discussed in the next section). We also assume that substances do not penetrate the dermis-epidermis interface, requiring zero vertical flux at $y = 0$.

For the other boundaries we will use Dirichlet boundary conditions. Far away from the wound, concentrations take their unwounded dermal value i.e. $c \to c_0$ as $x \to \infty$. Assuming that different biological processes occur within the subdermal tissue (since deep wounds are beyond the scope of our models), we stipulate the conditions $c = c_b$ at $y = y_b$, the wound base.

Initial conditions vary according to the model framework and roles of the corresponding variable. The natural initial values for most variables will be zero within the wound ($0 < x < L$) at onset, and their normal dermal values outside of the wound ($x > L$).

2.4 Fluxes

As mentioned earlier, the fluxes J_i for each variable have dependence on some of the other variables or their derivatives. It is through the J_i that we model the chemical processes of random diffusion, chemotaxis, haptotaxis and haptokinesis. The most general form for a flux is therefore

$$\vec{J_n} = \vec{J}_{random} + \vec{J}_{chemo} + \vec{J}_{h.kinesis} + \vec{J}_{h.kinesis} \tag{2.2}$$

To describe the random motion of substance n, we assume a flux of the form

$$\vec{J}_{random} = -D_n n^{\alpha} \nabla n \tag{2.3}$$

where D_n, the random-motility coefficient and α are positive constants. In some cases we will depart from the standard assumption of linear diffusion ($\alpha = 0$) for reasons which are discussed later.

For angiogenesis to be effective we require more than just random diffusion processes. $\vec{J}_{chemo}$ and $\vec{J}_{h.taxis}$ represent biased migration up density gradients. They take the form

$$\vec{J} = \chi(m) n \nabla m \tag{2.4}$$

where $m(\vec{x}, t)$ represents the concentration of the substance whose chemical gradient the substance n migrates up. The haptotactic/chemotactic coefficient is often taken to have the form

$$\chi(m) = \chi_0 (c + m)^{-\beta} \tag{2.5}$$

for constants $\chi_0, c, \beta \geq 0$, reflecting the assumption that chemotactic sensitivity decreases with increased concentration of m.

Haptokinesis is described as unbiased migration, mediated by the ECM. The corresponding flux will therefore take the form of random diffusion, but the rate of diffusion will be a function of the ECM density. Hence

$$\vec{J}_{h.kinesis} = -D(m)\nabla n \tag{2.6}$$

where D is some function that satisfies $D(0) = D(\infty) = 0$ as cells cannot move in the absence of ECM, and movement is restricted when it becomes too dense.

2.5 Kinetics

Each variable we include in our model will have some local kinetics associated with it. In the conservation equation, this is the term that allows creation or elimination of a quantity. When modelling concentration of substances in angiogenesis, we see that these are the terms that therefore represent proliferation and degradation. Various structures have been used to represent the kinetics with relative merits depending on which biological aspects of the process are being focussed on.

In general, these kinetics will be inter-dependent due to the interactive nature of the substances involved, generating interesting dynamics.

2.6 Continuous and deterministic vs. discrete and stochastic

The conservation equation is manifestly continuous, and with appropriate boundary conditions will produce deterministic results. However some models, [5, 6] have used a discretised form of the partial differential equations to develop a biased random-walk model. This has the advantage that one can follow the path of individual endothelial cells at the sprout tips and incorporate anastomosis, mitosis and branching explicitly into the model.

Anderson et al. [5] discretise their continuous system of equations using a finite difference approximation on a two-dimensional grid of discrete points. The dynamical equation for the sprout tips then have the form

$$n_{l,m}^{q+1} = n_{l,m}^{q}P_0 + n_{l+1,m}^{q}P_1 + n_{l-1,m}^{q}P_2 + n_{l,m+1}^{q}P_3 + n_{l,m-1}^{q}P_4 \tag{2.7}$$

where the subscripts specify the location on the grid and the superscripts are time-steps. The coefficients $P_0 - P_4$ can be though of as probabilities of being stationary or moving right, left, up or down respectively. The coefficients $P_1 - P_4$ have three components,

$$P_n = \text{random movement} + \text{chemotactic} + \text{haptotactic} \tag{2.8}$$

thus showing how the discrete system is linked to that of the continuous model.

This model will be reviewed when we come to focussing on discrete systems in Chapter 7.

Chapter 3

A Minimalist Model

The first model which we shall investigate [2] focuses on the densities of capillary tips and endothelial cells. Containing only two of the inter-dependent variables, this model is minimalist, but certainly non-trivial. Using a simpler model allows for detailed analytical investigation, which will demonstrate that the maximum densities of our variables depend on a very limited number of parameter groupings.

The maximum endothelial cell density is interpreted as a measure of the system's angiogenic ability, hence this modelling approach gives substantial insight into what factors may be responsible for angiogenesis. With this measure, one can then work towards finding the optimal means of increasing a system's angiogenic response.

3.1 The Mathematical Framework

The two inter-dependent variables, capillary tip and endothelial cell density, at position x and time t will be denoted respectively by $n(x,t)$ and $b(x,t)$. Assuming a slit excisional wound with negligible depth compared to length, we will work in one spatial dimension with the wound centre at $x = 0$. By assumed reflectional symmetry of the wound, we only need work with the semi-infinite domain $x \geq 0$.

We will construct the system of equations using the considerations from Chapter 2. The relative fluxes and kinetics of the two variables will be derived from biological considerations.

3.1.1 The capillary tip density equation

The flux that we use for the capillary tips needs to capture the phenomenologically reasonable supposition that the tips migrate via a random walk, with bias in the direction of decreasing blood vessel density i.e. towards the wound. Hence we take

$$J_n = J_{random} + J_{bias} = -D_1 \frac{\partial n}{\partial x} - D_2 n \frac{\partial b}{\partial x} \tag{3.1}$$

where D_1 and D_2 are positive diffusion coefficients.

Capillary tip kinetics need to take into account three processes namely tip branching, tip-tip anastomosis and tip-sprout anastomosis. It is assumed that at a given time, a fixed proportion λ_2 of existing sprouts will branch while the anastomosis terms will be non-linear and go like $-\lambda_3 n^2$ and $-\lambda_4 nb$ respectively. Hence our tip kinetics are given by

$$f(n,b) = \lambda_2 n - \lambda_3 n^2 - \lambda_4 nb \tag{3.2}$$

3.1.2 The endothelial cell density equation

As proposed in the biological model for angiogenesis, the capillary sprouts passively follow their leading tip. Hence the flux of the endothelial cell density is proportional to that of the capillary tips giving

$$J_b = -\lambda_5 \left(D_1 \frac{\partial n}{\partial x} - D_2 n \frac{\partial b}{\partial x} \right) \tag{3.3}$$

where λ_5 is the average number of endothelial cells in a capillary tip.

The kinetics of the endothelial cells involve three processes, each of which is represented by a term in the following.

$$g(n,b) = \lambda_6 \nu b(b_0 - b) + \lambda_6 \chi nb(b_1 - b) + \lambda_5(\lambda_3 n^2 + \lambda_4 nb) \tag{3.4}$$

The first logistic term represents cell proliferation with carrying capacity b_0 at a rate characterised by ν. We include a second logistic term proportional to n to represent the increased rate of remodelling observed in the immediate vicinity of a capillary tip. Finally, the third term balances the anastomosis terms in (3.2) as cell tips move in to the cell sprout category.

3.1.3 Initial and boundary conditions

A standard assumption is that initially there are neither capillaries nor tips in the wound space, and blood vessel density is at the normal unwounded level outside of the wound space. This model assumes a small (relative to b_0) initial distribution of active sprout tips at the wound edge since we are not explicitly considering mechanisms of initial endothelial cell stimulation. In mathematical form, our initial conditions are

$$n(x,0) = \begin{cases} 0 & x \in [0, L) \\ n_{init} & x \in [L, L+\zeta] \\ 0 & x \in (L+\zeta, \infty) \end{cases} \qquad b(x,0) = \begin{cases} 0 & x \in [0, L) \\ b_0 & x \in [L, \infty) \end{cases} \tag{3.5}$$

The boundary conditions are as mentioned in Chapter 2. Far from the wound centre the cell density takes its unwounded dermal value and there are no density tips. We also use the zero flux condition at the origin. Hence

$$n(\infty, t) = 0 \quad b(\infty, t) = b_0, \tag{3.6}$$

$$n_x(0,t) = b_x(0,t) = 0 \tag{3.7}$$

3.1.4 Non-dimensionalisation

An important technique in the modelling of biological systems is that of finding convenient scalings for the variables allowing certain parameters to be grouped together. This greatly simplifies the equations and lets us use characteristic scales as the unit quantity for each variable. For this specific model an outline of the rescaling is given in Appendix A, however in the proposed models to come, we will exclude this procedure for brevity.

We use the following rescaling:

$$\tilde{n} = \frac{n}{n_0}, \quad \tilde{b} = \frac{b}{b_0}, \quad \tilde{t} = \frac{t}{T}, \quad \tilde{x} = \frac{x}{L}. \tag{3.8}$$

The full set of equations for the system then becomes (dropping tildes for notational simplicity)

$$\frac{\partial n}{\partial t} = \underbrace{\frac{\partial}{\partial x}\left(C_1 \frac{\partial n}{\partial x}\right)}_{\text{diffusion}} + \underbrace{\frac{\partial}{\partial x}\left(C_2 n \frac{\partial b}{\partial x}\right)}_{\text{biased movement}} + \underbrace{f(n,b),}_{\text{tip kinetics}} \tag{3.9}$$

$$\frac{\partial b}{\partial t} = k_5 \frac{\partial}{\partial x} \underbrace{\left(C_1 \frac{\partial n}{\partial x} + C_2 n \frac{\partial b}{\partial x}\right)}_{\text{same flux}} + \underbrace{g(n,b)}_{\text{capillary kinetics}} \tag{3.10}$$

$$f(n,b) = k_2 n - k_3 n^2 - k_4 n b, \tag{3.11}$$

$$g(n,b) = \chi n \beta_1 b \left(1 - \frac{b}{\beta_1}\right) + \nu b(1-b) + k_5 k_3 n^2 \tag{3.12}$$

where the dimensionless parameters $C_1, C_2, k_2, k_3, k_4, k_5, \chi, \nu, \beta_1, \zeta$ and n_{init} are non-negative constants resulting from the rescalings of our original parameters. Definitions are given in Appendix A.

The rescaled initial and boundary conditions are simply given by (3.5) to (3.7) with $L = b_0 = 1$.

3.2 Simulation and Analysis

3.2.1 Homogeneous steady states of the system

Before we look into any simulations of the model, let us briefly consider the steady states (n_*, b_*) of the system, which satisfy $f(n_*, b_*) = g(n_*, b_*) = 0$. These are given by

$$(n_*, b_*) = (0,0), \ \ (0,1), \ \ (\frac{k_2}{k_3} = 1, 0) \tag{3.13}$$

The first two of these represent the wounded and unwounded steady states respectively. Assuming a healing wound, we require the former to be unstable and the latter to be stable. The third steady state is biologically irrelevant since a system of capillary tips without blood vessels is implausible. We choose parameters such that $k_2 = k_3$ and $k_4 > k_2$. The first of these conditions is motivated in

Appendix A, the second is considered in Section 3.2.3 where we show the condition is necessary for connectivity of the wounded and unwounded states.

To evaluate stability subject to spatially homogeneous perturbations, we calculate the Jacobian matrix

$$J = \begin{pmatrix} \frac{\partial f}{\partial n} & \frac{\partial f}{\partial b} \\ \frac{\partial g}{\partial n} & \frac{\partial g}{\partial b} \end{pmatrix} \tag{3.14}$$

evaluated at the stationary points.

We have

$$J|_{(0,0)} = \begin{pmatrix} k_2 & 0 \\ 0 & \nu \end{pmatrix}, \tag{3.15}$$

$$J|_{(0,1)} = \begin{pmatrix} k_2 - k_4 & 0 \\ \chi\beta_1(1 - \frac{1}{\beta_1}) & -\nu \end{pmatrix} \tag{3.16}$$

$$\text{and } J|_{(1,0)} = \begin{pmatrix} -k_2 & -k_4 \\ 2k_5k_2 & \chi\beta_1(1 - \frac{2}{\beta_1}) + \nu \end{pmatrix}. \tag{3.17}$$

Recall from the theory of dynamical systems that for stability we require $Re(\lambda_{1,2}) < 0$ where $\lambda_{1,2}$ are the eigenvalues of the J at the stationary points. If $Re(\lambda_{1,2}) > 0$ we have an unstable node/spiral and eigenvalues of opposite signs represent a saddle point (also unstable).

In the case of two dimensional matrices, calculating the determinant and trace suffices in providing us with this information. [1] The condition for stability is now $trJ < 0, detJ > 0$.

For (3.15) we have $trJ > 0, detJ > 0 \Rightarrow Re(\lambda_{\pm}) > 0 \Rightarrow (0,0)$ is unstable (as expected).

For (3.16) we have $trJ = k_2 - k_4 - \nu < 0$ upon choice of parameter $k_4 > k_2$. $detJ = \nu(k_4 - k_2) > 0$ hence $Re(\lambda_{\pm}) < 0$ which implies that (0,1), the unwounded (recovered) state is stable.

In (3.17) we have more complicated expressions however note that
$detJ = -k_2[\chi(\beta_1 - 2) + \nu - 2k_5k_4]$. We will always be using parameters such that the square bracketed factor is positive, and hence $(1,0)$ will be a saddle point (unstable as required).

3.2.2 A Simulation

The equations of this model constitute a set of non-linear coupled convective-diffusion equations with non-linear kinetics. They can be solved numerically by computer using an explicit numerical method. A simulation at time 23 days is given by Figure 3.1.

There are a number of features to note from these density profiles which compare to the biological description of the process. The peak in capillary tips is closely followed by the peak in blood vessel density as the substances move towards the wound centre. A near travelling wave profile exhibited by both variables has been observed from further simulations. We will define the 'structural unit'

[1] The eigenvalues are given by $\lambda_{\pm} = \frac{trJ \pm \sqrt{trJ^2 - 4detJ}}{2}$

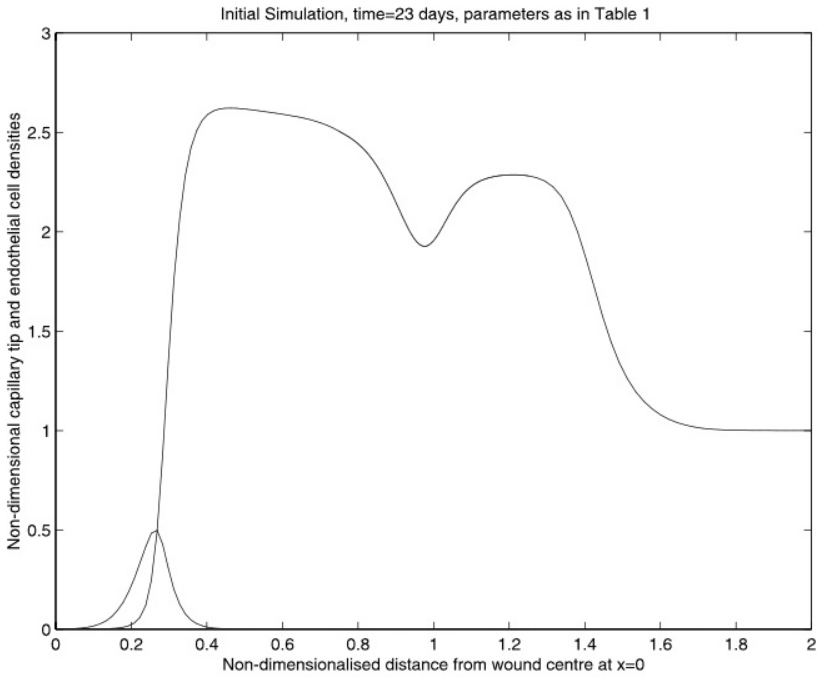

FIGURE 3.1: An initial simulation at time 23 days. Taken from [2].

as the capillary tip peak and endothelial cell front. The speed of the structural unit can be well approximated and will be discussed later.

Recall that the unwounded state $(0, 1)$ is the only stable steady state of the system, so we expect the system to settle down to this as $t \to \infty$. The simulation demonstrates that there is an elevated density of blood vessels in the wave back so $n \to 0$ much faster than $b \to 1$ for relatively large x. This is consistent with the biological model where it is understood that an increase in blood vessel density to normal dermal values is required for mending of the wound.

3.2.3 Travelling wave approach

We convert the system of PDEs into ODEs using the travelling wave coordinate $z = x + ct$ and transformed variables $N(z) = n(x, t), B(z) = b(x, t)$. The model equations become

$$C_1 N'' + C_2 (NB')' - cN' + f(N, B) = 0 \tag{3.18}$$

$$k_5 C_1 N'' + k_5 C_2 (NB')' - cB' + g(N, B) = 0 \tag{3.19}$$

where $'$ denotes $\frac{d}{dz}$.

The wave travels from the unwounded dermis to the unhealed wound so the boundary conditions are intuitively $B(\infty) = 1, B(-\infty) = N(\infty) = N(-\infty) = 0$. Linearising about the steady states $(0, 0)$ and $(0, 1)$ decouples equations (3.18) and (3.19) allowing for phase portrait analysis of N. Equation

(3.18) becomes

$$C_1N'' - cN' + k_2N = 0 \qquad \circlearrowleft (0,0) \tag{3.20}$$

$$C_1N'' - cN' + k_2N - k_4N = 0 \qquad \circlearrowleft (0,1) \tag{3.21}$$

We focus first on the phase portrait of N around the wounded steady state $(0,0)$. Let $D = N'$, then (3.18) becomes the following coupled pair of first order odes:

$$\begin{pmatrix} N' \\ D' \end{pmatrix} = \begin{pmatrix} 0 & 1 \\ -\frac{k_2}{C_1} & \frac{c}{C_1} \end{pmatrix} \begin{pmatrix} N \\ D \end{pmatrix} = A \begin{pmatrix} N \\ D \end{pmatrix} \tag{3.22}$$

Since we require that $N > 0$ we must have a node at the origin as opposed to a spiral. Theory from dynamical systems tells us that a necessary condition for this, is that both eigenvalues are real. Any imaginary part would contribute towards oscillations leading to a spiral form about the origin corresponding to unfeasible solutions for N.

The condition for real eigenvalues is equivalent to

$$trA^2 - 4detA \geq 0 \quad \Rightarrow \quad c^2 \geq 4k_2C_1 \tag{3.23}$$

This gives us a minimum wave speed of $c_{min} = 2\sqrt{k_2C_1}$.

In the neighbourhood of the unwounded steady state $(0,1)$ we have

$$\begin{pmatrix} N' \\ D' \end{pmatrix} = \begin{pmatrix} 0 & 1 \\ \frac{k_4-k_2}{C_1} & \frac{c}{C_1} \end{pmatrix} \begin{pmatrix} N \\ D \end{pmatrix} = B \begin{pmatrix} N \\ D \end{pmatrix} \tag{3.24}$$

Note that both eigenvalues for A are positive corresponding to an unstable node. For a travelling wave solution to exist, a heteroclinic trajectory must exist from the 'wounded equilibrium' $(0,0)$ to the 'dermal equilibrium' $(0,1)$ lying wholly in the biologically realistic region $N \geq 0, M \geq 0$. For this to be the case, we require at least one stable eigenvalue of B. Observe that $trB > 0$ and so to have a negative eigenvalue we require a saddle point i.e.

$$detB < 0 \Rightarrow k_4 > k_2 \tag{3.25}$$

This yields the parameter condition that was introduced earlier and justifies its inclusion into the model.

Note that this phase plane approach to the travelling wave solutions is separate from calculating the stability of the steady states to spatially homogeneous perturbations, to which the unwounded equilibrium state was stable.

3.2.4 Wave profile observations

From Figure 3.1 we noted that $n \to 0$ much faster than $b \to 1$. This was to be expected as one anticipates that there is a significant density of capillary tips only at, or near, the edge of the invading structural unit, but a raised concentration of blood vessels in the forming granulation tissue at,

and behind, the invading structural unit. We now look towards finding a (non-dimensionalised) characteristic lengthscale of the decay for endothelial cell density by looking at its waveback solution.

Linearising equation (3.19) about $(0, 1)$ gives

$$k_5 C_1 N'' - CB' + \nu B = 0. \tag{3.26}$$

The first term may be ignored under the observation that $N \to 0$ much faster than $B \to 1$ giving a simple ODE in B. Solving yields

$$B = 1 + E^{-\nu z/c} \tag{3.27}$$

where one may observe the characteristic lengthscale of decay $l = c/\nu$. Recall that ν characterises the rate of cell proliferation. Taking biologically reasonable parameter estimates we actually find that $l \sim O(10)$, much larger than the biologically realistic domain size (the wound length is $O(1)$). Thus a disadvantage to the travelling wave method is that the tail of the wave never forms on a biologically realistic domain size. Despite this, features of the travelling wave solutions prove to be useful approximations for many features of the actual 'wave-like' solutions to the full partial differential equations. Another simulation is given in Appendix A to demonstrate that with a sufficiently small l, near perfect travelling wave solutions are exhibited.

In the following section we analyse further the travelling wave solutions to provide approximations for the peak densities of capillary tips, and more importantly of the blood vessels, giving a measure of the system's angiogenic ability.

3.3 Detailed Travelling Wave Analysis - an asymptotic investigation

3.3.1 Further rescaling

We now look into finding the travelling wave solution in asymptotic form, expressing the solution as an expansion in some small parameter ϵ. With the PDEs in their current state, there is more than one small parameter, but with a convenient rescaling, we can group the parameters in such a way that only one grouping is small and the others are of $O(1)$.

The following rescaling

$$\tau = k_2 t, \quad y = \sqrt{\frac{k_2}{C_1}} x \tag{3.28}$$

gives

$$\begin{aligned} n_\tau &= n_{yy} + \rho_1 (n b_y)_y + (n - n^2) - \rho_2 n b, \\ b_\tau &= k_5 \left(n_{yy} + \rho_1 (n b_y)_y\right) + \left(\rho_3 \beta_1 n + \frac{\nu}{k_2}\right) b - \left(\rho_3 + \frac{\nu}{k_2}\right) b^2 + k_5 n^2 \end{aligned} \tag{3.29}$$

where $\rho_1 = \frac{C_2}{C_1} \sim O(1)$, $\rho_2 = \frac{k_4}{k_2} \sim O(1)$, $\rho_3 = \frac{\chi}{k_3} \sim O(1)$ and $\frac{\nu}{k_2} \sim O(10^{-3})$.

The original travelling wave coordinate is scaled as

$$z = x + ct = \sqrt{\frac{C_1}{k_2}}y + \frac{c}{k_2}\tau = \sqrt{\frac{C_1}{k_2}}\left(y + \frac{c}{\sqrt{C_1 k_2}}\tau\right).$$

Using the new travelling wave coordinate $\bar{z} = y + \bar{c}\tau$ we have $z = \sqrt{\frac{C_1}{k_2}}\bar{z}$ and $\bar{c} = \frac{c}{\sqrt{C_1 k_2}}$. Now the wave speed inequality (3.23) becomes $\bar{c} \geq 2$ and we can use $\bar{c}$ to define a small parameter

$$\epsilon = \frac{1}{\bar{c}^2} \leq \frac{1}{4}. \tag{3.30}$$

From this point on we shall now hypothesise that the structural unit moves at the minimum travelling wave speed so we shall take $\epsilon = \frac{1}{4}, \bar{c} = 2$. A discussion on this is given in Appendix A.

The small parameter grouping that arises in (3.29) is $\frac{\nu}{k_2}$. Since $\epsilon^4 \sim O(10^{-3})$ we can define $\rho_4 \sim O(1)$ and write $\frac{\nu}{k_2} = \rho_4\epsilon^4$. We are now in a position to rescale $\bar{z}$ based on ϵ and use the method of asymptotic matching to find solutions to the travelling wave equations.

3.3.2 Asymptotic Solutions

The travelling wave equations are derived from (3.29) using the new coordinate $\xi = \epsilon^{\frac{1}{2}}\bar{z}$ and writing $N(\xi) = n(y,t)$ and $B(\xi) = b(y,t)$.

They read

$$\epsilon N_{\xi\xi} + \rho_1\epsilon\left(NB_\xi\right)_\xi - N_\xi + (N - N^2) - \rho_2 NB = 0 \tag{3.31}$$

$$k_5\epsilon\left[N_{\xi\xi} + \rho_1\left(NB_\xi\right)_\xi\right] - B_\xi + (\rho_3\beta_1 N + \rho_4\epsilon^4)B - (\rho_3 N + \rho_4\epsilon^4)B^2 + k_5 N^2 = 0 \tag{3.32}$$

We will seek asymptotic solutions to these equations in the three regions as indicated by Figure 3.2. The solutions will then be matched, allowing us to develop insight into the wave structure.

3.3.2.1 Inner region

For the inner solution, we assume that $B, N \sim O(1)$. Using a standard expansion in ϵ we have

$$N = N_0 + \epsilon N_1 + \epsilon^2 N_2 + \cdots$$
$$B = B_0 + \epsilon B_1 + \epsilon^2 B_2 + \cdots$$

Substituting these into the wave equations, keeping only $O(1)$ terms and regarding $\frac{k_5}{\rho_3\beta_1}$ as asymptotically small we get the following set of coupled ordinary differential equations:

$$\frac{dN_0}{d\xi} = N_0(1 - N_0 - \rho_2 B_0) \tag{3.33}$$

$$\frac{dB_0}{d\xi} = N_0\rho_3\beta_1\left(1 - \frac{B_0}{\beta_1}\right) \tag{3.34}$$

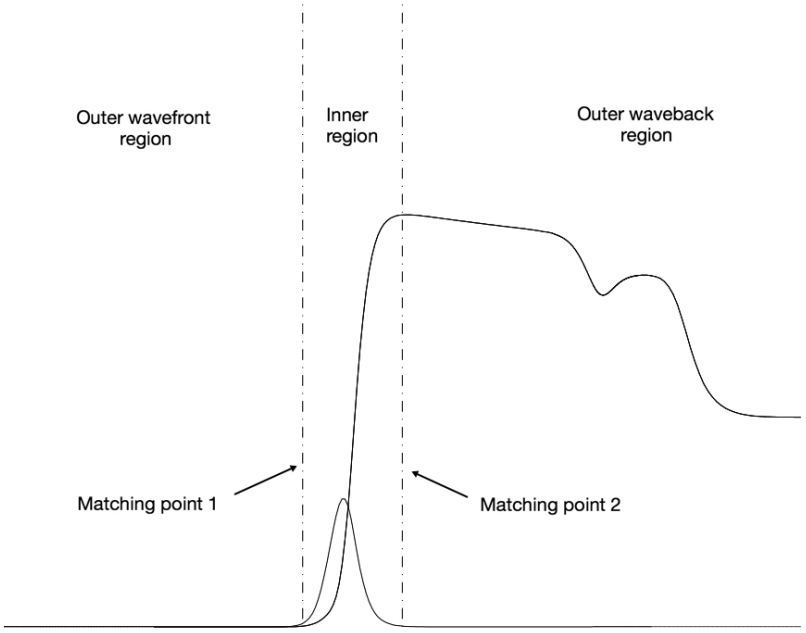

FIGURE 3.2: The three asymptotic regions of the travelling wave

Dividing these equations gives a first order ODE for N_0 in terms of B_0 which can be solved using an integrating factor of $\psi_0 = \left(\frac{B_0}{\beta_1 - B_0}\right)^{\frac{1}{\rho_3\beta_1}}$ to get

$$\boxed{N_0 = \frac{1}{\psi_0}[D + H(d, B_0)]} \tag{3.35}$$

where

$$H(a,b) = \int_a^b \frac{1-\rho_2 B_0}{\rho_3\beta_1 B_0\left(1-\frac{B_0}{\beta_1}\right)}\psi_9(B_0)dB_0 \tag{3.36}$$

and D, d are related constants with only one degree of freedom between them. For future use, we will define

$$\psi_k = \left(\frac{B_k}{\beta_1 - B_k}\right)^{\frac{1}{\rho_3\beta_1}} \tag{3.37}$$

Equation (3.36) can be simplified to give

$$\begin{aligned} H(a,b) =&(1-\rho_2\beta_1)\left[\left(\frac{b}{\beta_1-b}\right)^{\frac{1}{\rho_3\beta_1}} - \left(\frac{a}{\beta_1-a}\right)^{\frac{1}{\rho_3\beta_1}}\right] \\ &+\rho_2\beta_1\int_{\left(\frac{a}{\beta_1-a}\right)^{\frac{1}{\rho_3\beta_1}}}^{\left(\frac{b}{\beta_1-b}\right)^{\frac{1}{\rho_3\beta_1}}} \frac{du}{1+u^{\rho_3\beta_1}}, \end{aligned} \tag{3.38}$$

hence

$$H(B_i, B_j) = (1-\rho_2\beta_1)(\psi_j - \psi_i) + \rho_2\beta_1\int_{\psi_i}^{\psi_j}\frac{du}{1+u^{\rho_3\beta_1}}. \tag{3.39}$$

This will come in useful when we start to calculate maximum densities.

3.3.2.2 Outer waveback region

In the waveback region we have N very small and $B \to 1$ for $\xi \to \infty$. In order not to dominate the $\rho_4\epsilon^4$ terms in (3.32) we assume N is of order not more than ϵ^4 which yields expansions

$$N = \epsilon^4 N_0 + \epsilon^5 N_1 + \cdots$$
$$B = B_0 + \epsilon B_1 + \cdots$$

By the same procedure of substitution and keeping leading order terms, we get the dynamical equations

$$\frac{dN_0}{d\xi} = N_0(1 - \rho_2 B_0) \tag{3.40}$$
$$\frac{dB_0}{d\xi} = \rho_4\epsilon^4 B_0(1 - B_0) \tag{3.41}$$

and upon integrating,

$$\boxed{N_0 = K B_0^{\frac{1}{\rho_4\epsilon^4}} |1 - B_0|^{\frac{\rho_2 - 1}{\rho_4\epsilon^4}}} \tag{3.42}$$

3.3.2.3 Outer wavefront region

Here, both N and B are small. By similar argument to before take $N \sim O(\epsilon^4)$. When deciding upon a perturbative expansion for B, we need to consider to what power of ϵ would give us a non-trivial leading order. This is only the case when $B \sim O(\epsilon^5)$, hence take

$$N = \epsilon^4 N_0 + \epsilon^5 N_1 + \cdots$$
$$B = \epsilon^5 B_0 + \epsilon^6 B_1 + \cdots .$$

Substituting into (3.31), the leading order is ϵ^4 and yields $N_0' = N_0(1 + O(\epsilon))$. At leading order of ϵ^5, equation (3.32) yields $B_0' = k_5 N_0''(1 + O(\epsilon^4))$. Integrating, and noting boundary conditions as $\xi \to -\infty$ ($B_0 = N_0' = 0$) to determine the integration constant we have

$$\boxed{B_0 = k_5 N_0'(1 + O(\epsilon^4)) = k_5 N_0(1 + O(\epsilon))} \tag{3.43}$$

3.3.2.4 Matching of the solutions

We now have the asymptotic solutions in each of the three regions up to two constants, K and $D(d)$. It was noted previously that the function expansions undergo a structural change when the $\rho_4\epsilon^4$ terms are the same order as the $\rho_3\beta_1 N$ and $\rho_3 N$ terms in (3.32). So we will match, when these terms become equal to each other, i.e

$$|\rho_3 N(\beta_1 - B)| = |\rho_4\epsilon^4(1 - B)|. \tag{3.44}$$

Denote $B_{(i)}, N_{(i)}$ as the values of B and N at matching point i. The two matching points are labelled in Figure 3.2.

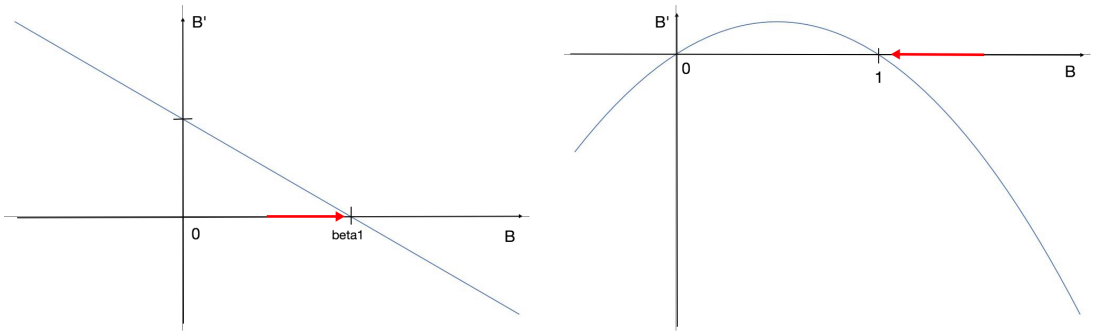

(A) inner region (B) outer waveback regin

FIGURE 3.3: Phase portraits of B in the inner and outer waveback regions

Finding $B_{(1)}$ and $N_{(1)}$ is straight-forward using the matching condition (3.44), combined with the inner and outer wavefront solutions (3.35), (3.43). From now on we take the integral limit of (3.35), $d = B_{(1)}$ and subsequently we can find D from the three equations in the three unknowns.

After some algebra

$$B_{(1)} = \frac{k_5\rho_4}{\rho_3\beta_1}\epsilon^5(1 + O(\epsilon)), \tag{3.45}$$

and hence $\psi_1^{\rho_3\beta_1} \sim O(\epsilon^5)$, which we will use in calculating the capillary tip density maximum. Note that ψ_1, ψ_2 correspond to $B_{(1)}, B_{(2)}$ respectively, not B_1, B_2.

Three equations of similar structure, now in the unknowns $(B_{(2)}, N_{(2)}, K)$ can be generated at the second matching point. Solving them analytically is too cumbersome, however we can make an important observation about $B_{(2)}$.

All numerical simulations have suggested that $1 < b_{max} < \beta_1$. Consider the turning points of B in the inner and outer waveback regions using the dynamical equations (3.34) and (3.41). Their phase portraits are sketched in Figure 3.3. Since we assume that B never reaches β_1, B will increase monotonically in the inner region until it reaches the matching point. It is clear from simulations that at this point we have $B > 1$ and so the second phase portrait indicates that from this point on, B will decrease onto its stable steady state of $B = 1$. Hence $B_{(2)}$ is actually the maximum value of B, (b_{max}) in our matched solution.

3.3.3 Density Maxima

We have essentially obtained the full travelling wave solution in asymptotic form. Using this, one can now qualify additional features of the wave profile. Specifically, we are interested in the maxima of the capillary tip and blood vessel densities, which will now be calculated.

3.3.3.1 Capillary tip density maximum

It is clear from numerical simulations that the capillary tip density maximum occurs within the inner region. Using (3.33) we see

$$\frac{dN_0}{d\xi} = 0 \quad \Rightarrow \quad N_0 = 1 - \rho_2 B_0 \tag{3.46}$$

giving the implicit equation for N_{max}:

$$N_{max} = 1 - \rho_2 B(N_{max}) \tag{3.47}$$

In the previous section we worked out $N(B)$ in the inner region to leading order, given by (3.35). Setting $B_* = B(N_{max})$ and the integration limit $d = B_{(1)}$ we have

$$\begin{aligned} 1 - \rho_2 B_* &= N(B_*) \\ &= \frac{1}{\psi_*}\left[O(\epsilon^4) + H(B_{(1)}, B_*)\right] \\ &= \frac{1}{\psi_*}\left[(1-\rho_2\beta_1)(\psi_* - \psi_1) + \rho_2\beta_1 \int_{\psi_1}^{\psi_*} \frac{du}{1+u^{\rho_3\beta_1}} + O(\epsilon^4)\right], \end{aligned} \tag{3.48}$$

where in the last line we have used (3.39). Rearranging and eliminating B_* for ψ_* gives

$$\int_0^{\psi_*} \frac{du}{1+u^{\rho_3\beta_1}} - \int_0^{\psi_1} \frac{du}{1+u^{\rho_3\beta_1}} = \frac{1-\rho_2\beta_1}{\rho_2\beta_1}\psi_1 + \frac{\psi_*}{1+\psi_*^{\rho_3\beta_1}} \tag{3.49}$$

Now make the ansatz that $\psi_*^{\rho_3\beta_3} \ll 1$ and recall that $\psi_1^{\rho_3\beta_1} \sim O(\epsilon^5)$. Then Taylor expanding the integrands and neglecting terms of order $\psi_*^{2\rho_3\beta_3}$, we can solve to get

$$\psi_*^{\rho_3\beta_1} = \left(\frac{\rho_3\beta_1 + 1}{\rho_2\rho_3\beta_1^2}\psi_1\right)^{\frac{\rho_3\beta_1}{\rho_3\beta_1+1}}. \tag{3.50}$$

and finally, the maximum capillary tip density

$$\begin{aligned} n_{max} &= 1 - \rho_2 B_* \\ &= 1 - \rho_2\left(\frac{\beta_1\psi_*^{\rho_3\beta_1}}{1+\psi_*^{\rho_3\beta_1}}\right) \\ &= 1 - \rho_2\beta_1\psi_*^{\rho_3\beta_1}\left(1 + O(\psi_*^{\rho_3\beta_1})\right) \end{aligned} \tag{3.51}$$

Of course this is only reliable if our ansatz is valid i.e if

$$\psi_*^{\rho_3\beta_1} = \left(\frac{\rho_3\beta_1+1}{\rho_2\rho_3\beta_1^2}\left(\frac{k_5\rho_4}{\rho_3\beta_1}\epsilon^5\right)^{\frac{1}{\rho_3\beta_1}}\right)^{\frac{\rho_3\beta_1}{\rho_3\beta_1+1}} \ll 1 \tag{3.52}$$

which does hold for biologically reasonable parameter values.

3.3.3.2 Endothelial cell density maximum

When analysing our asymptotic solutions we found that the endothelial cell density maximum is actually given by $B_{(2)}$. We can derive an implicit integral equation satisfied by ψ_2 from the matching condition and the inner solution evaluated at the matching point. It is given by

$$(1-\rho_2\beta_1)\psi_2 + \rho_2\beta_1\int_0^{\psi_2}\frac{dx}{1+x^{\rho_3\beta_1}} = \psi_1. \tag{3.53}$$

Thus from the definition of ψ_2, we have

$$b_{max} = B_{(2)} = \frac{\beta_1 \psi_2^{\rho_3 \beta_1}}{1 + \psi_2^{\rho_3 \beta_1}}.$$

3.3.4 Insights into angiogenesis

Before we embark on what this model tells us about angiogenesis, let us recall the important parameters that our results depend upon, and the processes/quantities they govern.

- C_1 : Capillary tip diffusive random motion
- C_2 : Capillary tip biased motion towards areas of reduced blood vessel density.
- k_2 : Strength of tip branching
- k_4 : Strength of anastomosis
- χ : Rate of capillary tip induced cell proliferation
- $\beta \left(= \frac{b_1}{b_0}\right)$: Ratio of carrying capacities of capillary tip induced cell proliferation and logistic remodelling cell proliferation.
- $k_5 \left(= \frac{\lambda_5 n_0}{b_0}\right)$: Ratio of endothelial cells at carrying capacity limits of tip density and remodelled cell density.
- ν : Rate of logistic remodelling

The first prediction from the model is the dependence of the wave speed solely on the rate of tip branching and random diffusion, given by $c = \sqrt{4C_1 k_2}$. Despite the model not evolving to a travelling wave on the biological domain, this has proven to be a very accurate predictor.

We then went on to find an approximation for the maximum capillary tip density given by equation (3.51). This has been confirmed to agree to a good approximation with the numerical simulations and so supports the use of a travelling wave structure for analysis. It demonstrates the interesting dependence of n_{max} on a single parameter grouping given by $\rho_2 \beta_1 \psi_*^{\rho_3 \beta_1}$ and how the reduction of this increases capillary tip density.

The most useful result however, is that of b_{max}, representing a system's angiogenic ability and ability to supply nutrients to the wound healing structural unit. Consequently we now look into specific changes of the angiogenic system that can be made to maximally increase blood vessel formation.

From equation (3.53), one can conduct a detailed perturbative expansion for $B_{(2)}$ in ψ_1 to give

$$b_{max} = \frac{\beta_1 \psi^{\rho_3 \beta_1}}{1 + \psi^{\rho_3 \beta_1}} + O(\psi_1) \tag{3.54}$$

where ψ satisfies

$$\frac{1}{\psi} \int_0^{\psi} \frac{dx}{1 + x^{\rho_3 \beta_1}} = \frac{\rho_2 \beta_1 - 1}{\rho_2 \beta_1}$$

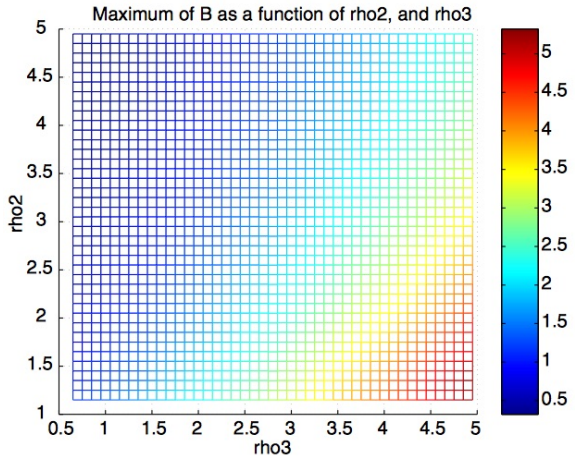

FIGURE 3.4: A density plot of Bmax varied with rho2 and rho3. Taken from [2].

The important aspect to note here is that b_{max} is primarily dependent on the parameter groupings $\beta_1, \rho_2\beta_1$ and $\rho_3\beta_1$. It is most likely not empirically possible to change parameters that are purely functions of carrying capacities, hence we will assume β and k_5 to be fixed. We will also only consider variations induced by manipulating the angiogenic system such that

$$\delta\left(\frac{k_5 k_4}{\chi}\right) \ll \beta_1 = \beta + \frac{k_5 k_5}{\chi}, \tag{3.55}$$

hence we consider not the variation of β_1.

Consider the dependence then of b_{max} on $\rho_2 \left(= \frac{k_4}{k_2}\right)$ and $\rho_3 \left(= \frac{\chi}{k_2}\right)$. It is straightforward to show from (3.54) that b_{max} is monotonically increasing in ρ_3 and monotonically decreasing in ρ_2. In other words stimulation of capillary tip induced endothelial cell proliferation increases b_{max}, whereas stimulation of anastomosis decreases b_{max}. Note also the independence of b_{max} from ν, suggesting the non-intuitive result that an increased rate of cell remodelling in the system will not increase the strength of angiogenic response.

The dependence of b_{max} on parameters ρ_2 and ρ_3 has been plotted in Figure 3.4 using computational methods on equation (3.53). This agrees nicely with our predictions, and demonstrates the relative sensitivity of b_{max} on the two parameters.

Consider now an angiogenic scenario, where we are interested in making specific changes in order to maximally increase blood vessel formation. Growth factors can be added to the system to alter cell motility and proliferation rates. Suppose we use a growth factor which uniformly stimulates proliferation for all cell types giving us the scaling $k_2 \to \Phi k_2, \chi \to \Phi\chi, \nu \to \Phi\nu$ for $\Phi > 1$. This gives $\rho_2 \to \frac{\rho_2}{\Phi}, \rho_3 \to \rho_3$, a desirable effect.

However suppose we use a cell specific factor that preferentially stimulates cells other than those constituting the capillary tips, giving us the scaling $k_2 \to k_2, \chi \to \Phi\chi$. Then $\rho_2 \to \rho_2, \rho_3 \to \Phi\rho_3$, another desirable effect. Clearly the merits of the two growth factors depend on the relative sensitivity

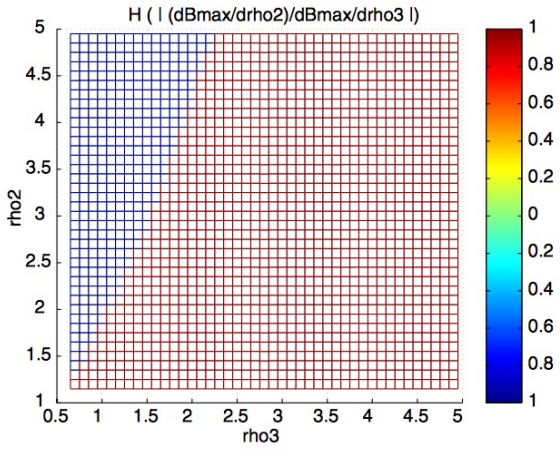

FIGURE 3.5: Evaluating the parameter range in which S is greater than/less than one. Taken from [2].

of b_{max} on ρ_2 and ρ_3. This can be determined by evaluating

$$S \overset{def}{=} \left| \frac{\partial B/\partial \rho_2}{\partial B/\partial \rho_3} \right|. \tag{3.56}$$

Then for $S \leq 1, b_{max}$ is more sensitive to ρ_3, and so the second growth factor mentioned would be a more beneficial treatment for the wound. Figure 3.5 shows the parameter range for which $S \leq 1$. We can deduce that should there be high levels of anastomosis (k_4) and/or low levels of proliferation in the vicinity of capillary tips (χ), then the preferential proliferative stimulation of cells excluding those at the capillary tips induces a greater angiogenic response.

In the following chapter we take a different approach to the modelling by including the ECM and its interactions with the endothelial cells.

Chapter 4

Regulatory Roles of the Extracellular Matrix

The previous model was built on the very simple framework of two variables, allowing us to perform detailed analysis of the system. It was however limited in its representation of angiogenesis, since there are many other varying factors that were not included. The ECM in particular plays an important role in regulating cell movement (random and directed) and proliferation. A model to include the interactions between the ECM and the endothelial cells has been proposed in the literature [3], which we shall review and discuss in this chapter.

4.1 The New Model

We wish to focus our attention mainly towards the interaction between the endothelial cells and the ECM, so the model has been restricted to use only one variable to represent the cell sprouts and tips together. Let $n(x,t), m(x,t)$ denote the endothelial cell density and ECM density respectively, at position x from the centre of the wound and time t post wounding. We shall use the same one dimensional domain for the cut as previously.

To determine the fluxes and kinetics for each variable, we consider the following fundamental interactions between the cells and the ECM during wound angiogenesis.

- **Haptokinesis** : This defines the unbiased (random) migration of the cells mediated by the ECM. This is represented by the cell flux $J_{kinesis} = -D(m)n_x$, with haptokinetic coefficient $D(m) = D_0 m(K_D^2 + m^2)^{-1}$. This suggests that the cells cannot move in the absence of ECM and become restricted when it becomes too dense. K_D is the optimum ECM density for cell movement. Note the corresponding diffusion coefficient in the previous model is D_1 which was restricted as being constant.

- **Haptotaxis** : This defines the biased migration of cells up ECM density gradients and is represented by flux $J_{taxis} = C(m)nm_x$. The haptotactic coefficient has been derived as $C(m) = C_0(K_C + m)^{-2}$.
- **Cell proliferation** : this is now dependent on the ECM density so the cell kinetics take the form $f(n, m) = [A(m) - Bn]n$ where $A(m)$ is the cell proliferation rate and we take this to have the same form as $D(m)$ with an optimum ECM density for cell proliferation K_A.
- **Production and degradation of ECM by cells** : It is the cells that manage the ECM density. They give ECM kinetics of $g(n, m) = (P - Qm)n$.

Along with standard boundary and initial conditions which are mentioned below, this is all the information we need to generate our system of equations, stemming from the conservation equations (2.1) corresponding to each variable.

The system is given by

$$n_t + [C(m)nm_x - D(m)n_x]_x = [A(m) - B(n)n] = f(n, m) \tag{4.1}$$

$$m_t = (P - Qm)n = g(n, m) \tag{4.2}$$

Take the intuitive initial and boundary conditions

$$n_x(0, t) = m_x(0, t) = 0, \quad n(x, t) \to n_0, \ \ m(x, t) \to m_0 \text{ as } x \to \infty.$$

$$n(x, 0) = \begin{cases} 0 & x \leq L \\ n_0 & x > L \end{cases}, \qquad m(x, 0) = \begin{cases} m_{init} & x \leq L \\ m_0 & x > L, \end{cases}$$

where n_0, m_0 are the unwounded dermal values and m_{init} is the low level of ECM initially at the wound site. This is due to the early deposition of provisional matrix; this process is not in the scope of the model.

4.2 Simulation and Analysis

4.2.1 Initial Observations

In a similar way to the analysis of the previous model, we can work with phase portraits to determine the stability of equilibrium points. One can readily show there exists a continuum of 'acellular' unstable states $(0, m)$ for any m and a stable state in which $n = A(m)/B$ and $m = P/Q$. In order for this to represent the 'healed' state, we set this equal to (n_0, m_0) extracting two degrees of freedom.

We transform the variables into dimensionless quantities using suitable scalings such that unit time is one day, unit length is the characteristic wound length and unit of chemical density is equal to its corresponding unwounded dermal value. Introducing scaled parameters accordingly give the following

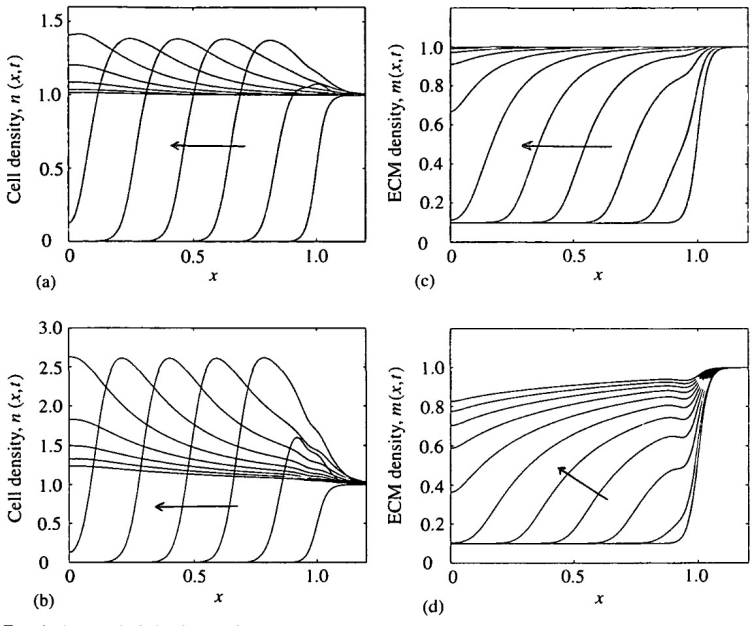

FIGURE 4.1: Numerical simulations at ten successive unit time intervals. The parameter variation from (a,c) to (b,d) is a decrease in ϵ to a fifth of its original value, representing slower ECM kinetics. Taken from [3].

dynamical equations:

$$n_t + (\chi(m)nm_x - D(m)n_x)_x = (\alpha(m) - \beta n)\, n \tag{4.3}$$

$$m_t = \epsilon(1-m)n. \tag{4.4}$$

Note the use of ϵ for the parameter in (4.4). This represents the rate of ECM remodelling which happens at a much slower rate than cell proliferation, so we can assume that it is small. Recall that finding a small parameter is useful for asymptotic methods of analysis.

From the numerical simulations in Figure 4.1, one can observe the wave like structure of the angiogenic response, propagating into the wound centre, in consistency with results in Chapter 3. Particular features of the dynamics to note are:

- the cell density peaks at a value higher than its unwounded level, before settling down to the steady state. This agrees with our understanding that there is an elevated blood vessel density throughout the wound site to help with tissue repair and to deliver extra nutrients to the cells already in the wound.
- the ECM density increases monotonically to its dermal value.
- it is after an initial transient and before reaching the wound centre that the profiles evolve with approximately constant form and speed (wave-like structure).
- the cell density gradients are steeper in the wave front than in the wave back.
- slowing the ECM kinetics seems to allow for a higher density of blood vessels to propagate towards the wound centre.

4.2.2 The Wavefront and the Fisher Equation

Prompted by the wave like nature in the simulations, we will again assume a travelling wave form and transform the dynamical equations into a system of ordinary differential equations using the wave coordinate $z = x + ct$. We take $c > 0$ which yields a 'left moving' wave as required. The equations read

$$cN' + [\chi(M)NM' - D(M)N']' = [\alpha(M) - N]N \tag{4.5}$$

$$cM' = \epsilon(1 - M)N, \tag{4.6}$$

where ' denotes differentiation with respect to z.

In an analogous way to the derivation of (3.23), one can show using phase plane analysis and the requirement of a heteroclinic trajectory from the 'wounded' equilibrium to the 'dermal' equilibrium that the wave speed c must satisfy

$$c \geq c_{min} = 2\sqrt{D(m_{init})\alpha(m_{init})}. \tag{4.7}$$

Thus the theoretical minimum wave speed solely has dependence on the haptokinetic and proliferation parameters. Note the independence of c_{min} on the haptotactic parameter χ due to its nonlinearity in equation (4.5). The effects of haptotaxis on the wave speed are investigated using numerical methods in the next section.

We can use asymptotic methods as in the previous chapter to find approximations to the wave solution. The boundary conditions for the wave profiles are given by $M \to m_{init}, N \to 0$ as $z \to -\infty$ and $M, N \to 1$ as $z \to \infty$. From equation (4.6) we see that to leading order in the wavefront, $M = m_{init}$ and hence equation (4.5) becomes

$$cN' = D(m_{init})N'' + [\alpha(m_{init}) - \beta N]N, \tag{4.8}$$

the Fisher equation, which has been widely studied in the literature. We shall review some of its properties and solutions [7].

First let us reduce equation (4.8) using the rescaling

$$u = \frac{\beta}{\alpha(m_{init})}N, \quad \hat{t} = \alpha(m_{init})t, \quad \hat{x} = \sqrt{\frac{\alpha(m_{init})}{D}}x, \quad \hat{z} = \hat{x} + c\hat{t}. \tag{4.9}$$

Dropping the hats gives the Fisher equation in its raw form:

$$u'' - cu' + u(1 - u) = 0 \tag{4.10}$$

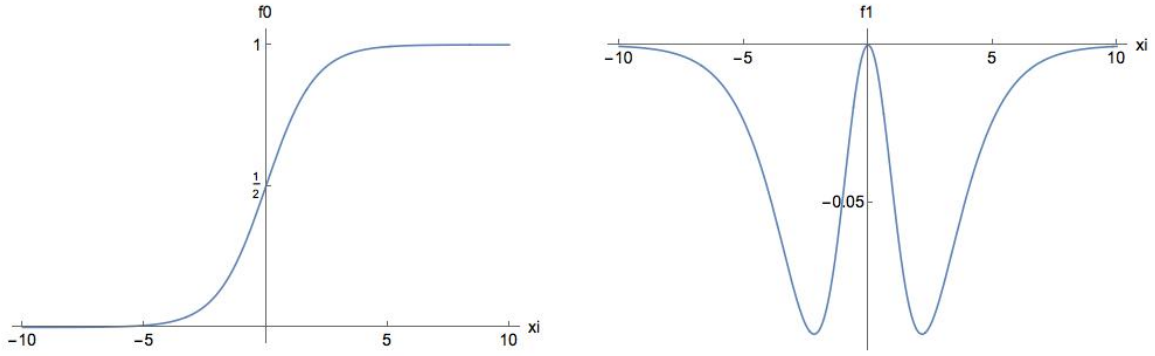

FIGURE 4.2: The first two orders of the asymptotic solution to the Fisher equation

In our case, the wavefront solution satisfies

$$\lim_{z\to-\infty} u(z) = 0 \quad \text{representing the wounded unstable state} \tag{4.11}$$

$$\lim_{z\to\infty} u(z) = 1 \quad \text{representing the healed stable state} \tag{4.12}$$

Note that wave solutions are invariant to any shift in the origin of the coordinate system. Hence we may chose the origin to satisfy $u(0) = 1/2$. The trick now is to introduce a change of variables in the vicinity of the front, in such a way that we can Taylor expand about the small parameter $\epsilon = 1/c^2$. We use the transformation $u(z) = f(\xi)$ where $\xi = \epsilon^{\frac{1}{2}} z$.

Equation (4.10) becomes

$$\epsilon f'' - f' + f(1-f) \tag{4.13}$$

and we are now in a position to write f as a perturbation series in ϵ, substitute back in and solve.

Writing

$$f(\xi;\epsilon) = f_0(\xi) + \epsilon f_1(\xi) + \cdots, \tag{4.14}$$

substituting into equation (4.13) and equating the first two powers of ϵ we get

$$O(1): \quad f_0' = f_0(1-f_0) \tag{4.15}$$

$$O(2): \quad f_1' - (1-2f_0)f_1 = f_0'' \tag{4.16}$$

These can be readily solved using the boundary conditions

$$f_0(0) = 1/2, \;\; f_0(-\infty) = 0, \;\; f_0(\infty) = 1, \;\; f_1(0) = 0 \text{ and } f_1(\pm\infty) = 0$$

to give

$$f_0 = (1+e^{-\xi})^{-1} \tag{4.17}$$

$$f_1 = e^{-\xi}(1+e^{-\xi})^2 \log(4e^{-\xi}(1+e^{-\xi})^2) \tag{4.18}$$

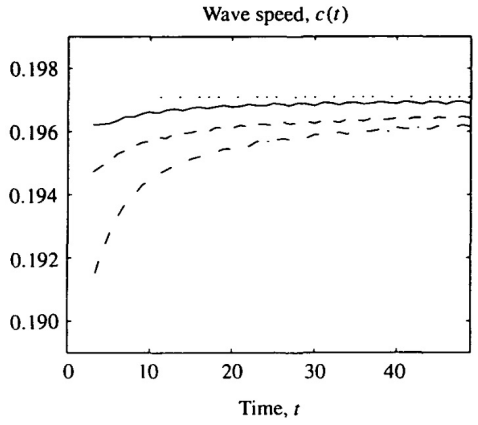

FIGURE 4.3: Evolution of the speed of angiogenesis on an extended biological domain. Calculations of speed have come from the model equations (4.3) and (4.4). The separate lines represent different values of χ: solid line - $\chi = 0$, dashed line below - $\chi = 0.001$, lowest dashed line - $\chi = 0.005$. The faint dotted line is $c = c_{min} = 0.197$.

which are both plotted in Figure 4.2. Values of f_1 are small in magnitude compared to f_0, so along with a factor of ϵ, this first order correction has little significance and hence $u(z) = f_0(z/c)$ suffices as a very good approximation to the solution.

An interesting property to consider is the 'steepness' of the wavefront. We will define this as the maximum value of $u'(z)$ which we can find from calculating the inflexion point of the wave (where $u''(z) = 0$). This occurs at $z = 0$ and it is straightforward to show from equations (4.14) to (4.16) that

$$u'(0) = \frac{1}{4c} + O\left(\frac{1}{c^2}\right) \tag{4.19}$$

So to a good approximation, the steepness of the wavefront is inversely proportional to the wave speed. This gives useful insight to the structural unit of endothelial cells. A faster moving structural unit will have a flatter wavefront of endothelial cells.

4.3 The Effect of Haptotaxis

The existence of travelling wave solutions is a conjecture rather than a certainty, based on the apparently stable wave-like forms that arise from numerically solving the partial differential equations (4.1) and (4.2). Though it is a good approximation, it does not take into account the effect of haptotaxis, due the non-linearity of the haptotactic flux term. We gain insight into these effects by analysing simulations of the model equations for various values of χ, the haptotactic coefficient. We extend the biological domain to allow travelling waves to develop to full form and settle onto some wave speed which we measure.

Figure 4.3 supports our conjecture that we can approximate angiogenesis with a travelling wave solution, since we see that the numerical solutions evolve towards the constant speed, predicted by c_{min}. Note that increasing the value of χ slows down the evolution towards this travelling wave solution

with speed c_{min}. Thus we have the counter-intuitive result that haptotaxis elicits cell movement away from the wound centre, thereby decelerating the angiogenic process. This is, however, yet to be tested experimentally with a suitable *in vitro* study.

Chapter 5

Unsuccessful Wound Healing

It is important to consider models where wound healing is not necessarily successful, in view of gaining insight into which parameters have most influence on the success of the angiogenic response. Generating a simulation for unsuccessful healing also allows us to interfere at certain times with parameter changes to represent application of a particular treatment to the wound. Experimenting with parameter values can lead to a more accurate understanding of what treatments for wound healing should provide in the way of growth factors.

Due to the complexity of angiogenesis there are several variables which we should take into account when considering healing prospects. Experimental results indicate that growth and development of the structural unit are controlled by mechanisms involving oxygen concentration within the tissue, together with various macrophage-derived growth-factors (MDGFs). MDGFs stimulate the endothelial cells of neighbouring blood vessels to become involved in the process. The response of the endothelial cells is a chemotactic one, hence the presence of macrophages in the wound site is vital for progress of the structural unit.

Having limited ourselves to two-variable models thus far, we now move on to include various other factors which play a part in angiogenesis.

5.1 A More Involved Model

The model we shall review [1] involves a total of six inter-dependent variables contributing in unique ways to the process of angiogenesis. We mention each one below, along with a brief explanation of its roles.

- **Capillary tips**: As with previous models, the tips exhibit a small degree of random motion mediated by the ECM. We also assume a chemotactic flux up the chemical gradient of chemoattractant, proportional to the ECM gradient. Kinetics will again be modelled upon tip branching and anastomosis.

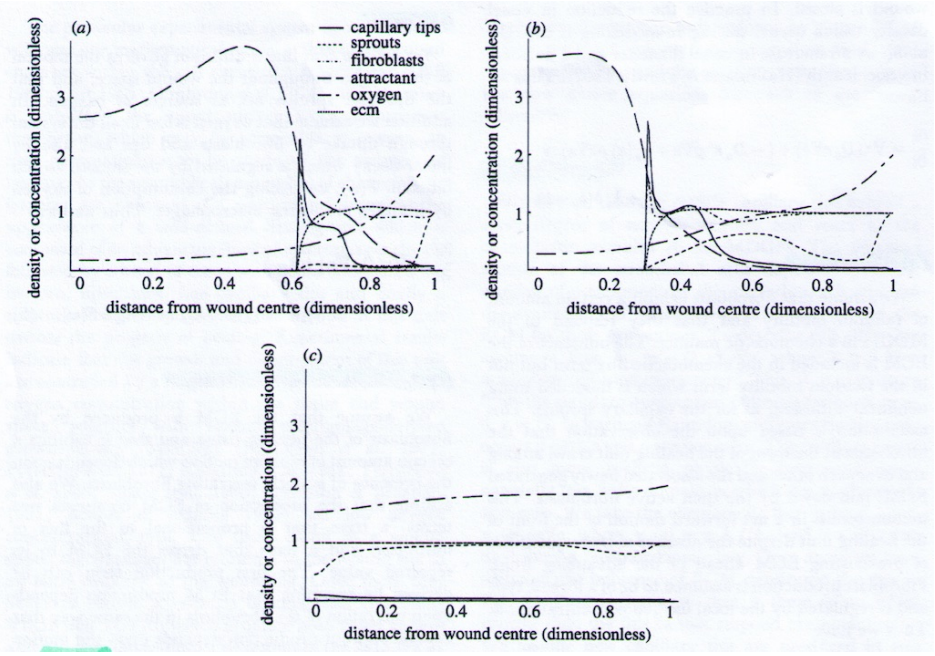

FIGURE 5.1: A simulation representing successful healing of the wound. As with previous models, observe the propagation of the structural unit toward the wound centre in (a) and (b). The sprout density then evolves to a uniform profile indicating full healing. Variables are plotted at times $t = 10, 15, 30$. Taken from [1].

- **Capillary sprouts**: Sprout motion is not independent of tip motion. We include a logistic term to describe the re-modelling of the capillary network.
- **Chemoattractant (MDGFs)**: We assume linear diffusion of the chemoattractant. It must be noted that the macrophages do not produce the chemoattractant if the oxygen concentration is either too high or too low. Hence a smoothed out switch function is included in the kinetics, which only allow creation of MDGFs for oxygen concentrations within a certain bracket.
- **Fibroblasts** : These respond to the MDGFs in a chemotactic manner provided there is ECM present. Fibroblasts undergo logistic growth.
- **Oxygen**: Tips and sprouts act as sources of oxygen. The oxygen is taken up by fibroblasts and decays through consumption by the macrophages to produce MDGFs.
- **ECM**: This is synthesised by the fibroblasts and mediates the migration of the endothelial cells.

A system of six coupled partial differential equations is proposed as a model (details given in [1]). We will focus simply on the results and applications to wound healing. Three simulations were generated corresponding to three distinct wound healing scenarios. Parameters were varied to generate (i) successful healing of the wound, (ii) unsuccessful healing of the wound and (iii) successful healing following case (ii) after a particular treatment has been applied. Investigation into parameter variations for subsequent healing will help us understand how best to intervene with a wound that has failed to heal on its own.

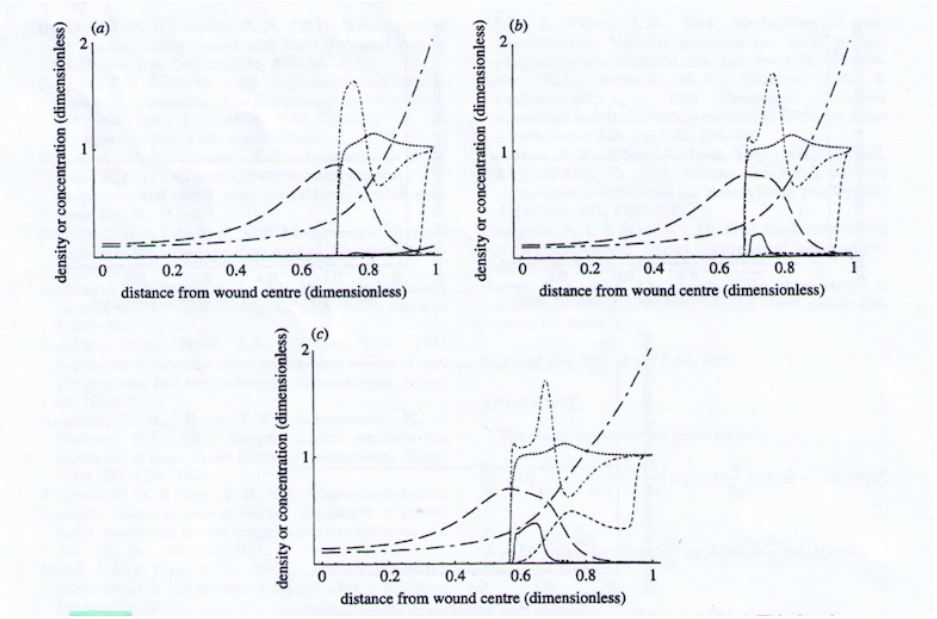

FIGURE 5.2: A simulation representing unsuccessful healing having decreased the parameters governing tip and attractant production. Note the reduced levels of oxygen at early times in the wound site and the cessation of the structural unit. Taken from [1].

5.2 Simulations

Case (i)

Parameters were chosen sensibly to correspond to a strong angiogenic response, stimulating the formation and propagation of a structural unit, into the wound centre. The simulation is given in Figure 5.1. We see that by $t = 30$ the wound has healed whereby the sprout and oxygen densities have evolved to near uniform profiles.

Case (ii)

Simulations showed that the reduction of two key factors can individually halt the propagation of the structural unit, thereby causing unsuccessful healing. They were found to be the rate of tip production and failure of the chemoattractant to form a sufficient gradient as a result of suppressed rate of attractant production. The migration of the structural unit relies upon chemotaxis, so without a strong enough chemical gradient to move up, the wave halts.

This agrees well with observed experimental and clinical observations. It has been observed [8] that inspired oxygen concentrations affect the rate and density of capillary growth, and when the attractant gradient is destroyed, capillary growth ceases. Ulcers developing in the wound tissue is often a cause of failure to form a sufficient chemoattractant gradient.

Case (iii)

The simulation generated in Figure 5.3 has used an initial distribution of the failed response (Figure 5.2, (c)) but reverted back to the original parameters selected in Figure 5.1. This is equivalent to a particular treatment being applied to the unhealed wound which stimulates the rate of tip and MDGF

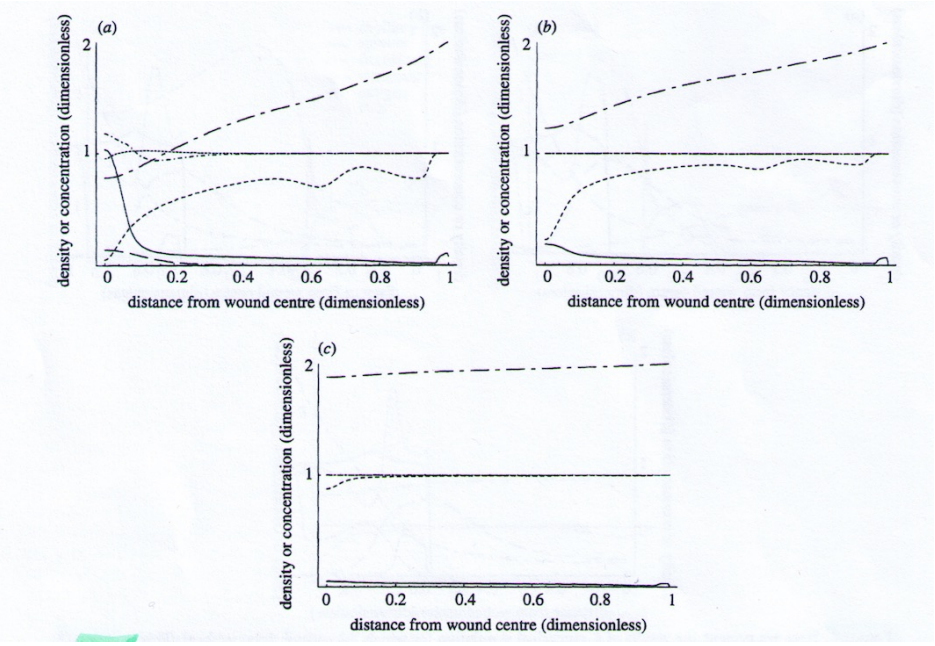

FIGURE 5.3: A simulation having taken an initial distribution of (c) from Figure 5.2 but reverting back to the parameter selection used in Figure 5.1. Taken from [1].

production. Fortunately, it can be seen from the simulation that the migration of the structural unit is reactivated and the system evolves towards the healed steady state.

The inclusion of many variables into this model gives it a lot of scope further numerical experiments. Parameters and initial conditions can be manipulated to represent specific cases and provide simulations for further analysis. This model can thus offer a number of possible explanations as to why a wound fails to heal and various mechanisms that may be employed to enhance healing.

Chapter 6

Extension to Multiple Dimensions

So far, we have only worked with a one dimensional domain to represent the wound and the body's angiogenic response. The corresponding models are limited due to the fact that a significant component of dermal healing proceeds from the base of the wound. A useful extension therefore, would be the inclusion of wound depth as a positional variable.

In this chapter, we will also consider a model for tumour induced angiogenesis. Despite being stimulated by different means, the process of angiogenesis itself has almost identical properties, and so these models will prove to be insightful for wound healing.

6.1 Inclusion of Wound Depth

The model proposed in Chapter 4 can easily be extended to two dimensions by incorporating wound depth, represented by $y \in [0, y_b]$. The mathematical domain is now given by $[0, \infty) \times [0, y_b]$. A diagram of the biological domain is given in Figure 2.1.

When extended to multiple dimensions, the non-dimensionalised cell flux term becomes

$$\vec{J} = (J_1, J_2)^T = \chi(m) n \nabla m - D(m) \nabla n, \tag{6.1}$$

representing haptotaxis and haptokinesis.

We will assume the Neumann boundary conditions of zero flux at $x = 0$ (imposed by symmetry) and at $y = 0$ (assuming that neither the cells nor ECM can penetrate the dermis-epidermis surface). This implies that $\vec{n}.\vec{J} = 0$ where $\vec{n}$ is the appropriate outward normal vector. At the wound base we will assume different biological processes are occurring which are not incorporated into this model, so take the Dirichlet boundary conditions of constant n and m equal to n_b and m_b respectively. Our final 'boundary' is at infinity, where we impose the standard conditions $n, m \to 1$ (the unwounded dermal values) as $x \to \infty$.

The initial conditions are the same as for the 1D model: $(n, m) = (0, m_{init})$ throughout the wound, $(n, m) = (1, 1)$ elsewhere in the domain.

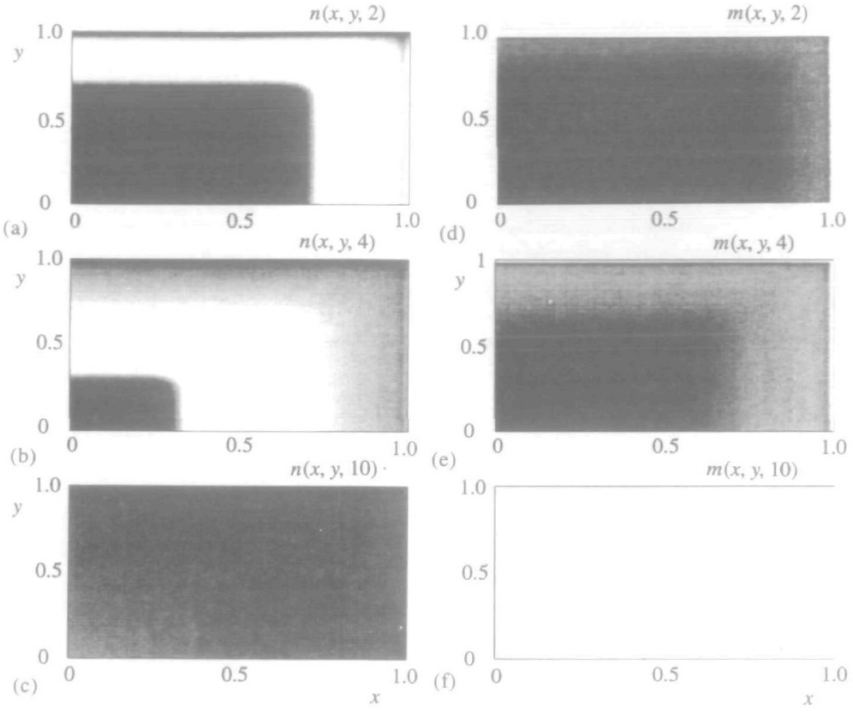

FIGURE 6.1: Simulations of the two dimensional model, illustrating propagation of cells and ECM into the wound. Higher densities are represented by lighter shading. Taken from [3].

Using the conservation equations with this flux and the same local kinetics f, g as for the one dimensional model we arrive at the equations

$$n_t + \nabla.\vec{J} = f(n, m) \tag{6.2}$$

$$m_t = g(n, m) \tag{6.3}$$

which have been solved numerically to give the density plots in Figure 6.1.

We observe that the accumulation of ECM follows the peak in the wave of endothelial cells, which propagates towards the wound centre - a similar feature to the 1D case. Note however the zone of interference which lies in a narrow region around the line $y = x$. Here there is a small relative increase in n and a decrease in m compared to the 1D solutions.

In this simulation, the depth of the wound has been given the same magnitude as the wounds characteristic length. A more realistic geometry for the wound would be to take $y_b \ll L$. Interestingly, simulations for varying wound depth [3] suggested that the wave speed does not depend on the depth/breadth ratio.

6.2 A Model for Tumour-Induced Angiogenesis

As previously mentioned, many models for tumour-induced angiogenesis are applicable to angiogenesis in wound healing due to the similar processes and chemicals involved. Here we look at a model which

will help us examine the relative importance of chemotaxis and haptotaxis in angiogenesis. In this system, the chemotaxis is induced by tumour angiogenic factors (TAF) which are supplied by the solid tumour. Haptotaxis is mediated by the presence of fibronectin within the ECM.

We denote the endothelial-cell density by n, the TAF concentration by c and the fibronectin concentration by f. For the chemotactic function χ, we choose a receptor-kinetic law of the form

$$\chi(c) = \chi_0 \frac{k_1}{k_1 + c} \tag{6.4}$$

reflecting the decrease in sensitivity of the cells to chemotaxis as the TAF concentration increases. We will take the haptotactic coefficient ρ_0 to be constant. Inclusion of these processes with random diffusion, we get the endothelial cell density flux

$$\vec{J_n} = -D_n \nabla n + \chi(c) n \nabla c + \rho_0 n \nabla f. \tag{6.5}$$

In this model we will focus attention on the endothelial cells at the sprout tips where no proliferation occurs. They also have a relatively long half-life, hence we shall omit the usual kinetics included for the endothelial cells, giving the simplified dynamical equation:

$$n_t + \nabla . \vec{J_n} = 0 \tag{6.6}$$

Fibronectin, a glycoprotein of the ECM, is present in most mammalian tissue and is produced and taken up by the endothelial cells. The production and uptake is modelled by

$$f_t = \omega n - \nu n f. \tag{6.7}$$

The initial event of tumour-induced angiogenesis is secretion of TAF by the tumour, providing an initial concentration profile of c. The endothelial cells respond to the steady state gradient and as they migrate across the ECM, there is some uptake of TAF by the cells, modelled by

$$c_t = -\lambda n c. \tag{6.8}$$

After performing a suitable rescaling which we omit for brevity, the non-dimensional dynamical equations read

$$n_t = D\nabla^2 n - \nabla . \left(\frac{\chi}{1 + \alpha c} n \nabla c \right) - \nabla . (\rho n \nabla f), \tag{6.9}$$

$$f_t = \beta n - \gamma n f \tag{6.10}$$

$$c_t = -\eta n c. \tag{6.11}$$

The domain will be a square of side L (rescaled to 1) representing a square of corneal tissue. Take the origin to be such that the domain is $(x, y) \in [0, 1] \times [0, 1]$. We assume that cells remain within the domain of the tissue, therefore the no-flux boundary condition $\vec{\zeta}.\vec{J_n}$=0 is imposed on the boundaries of the square where $\vec{\zeta}$ is the appropriate outward unit normal vector.

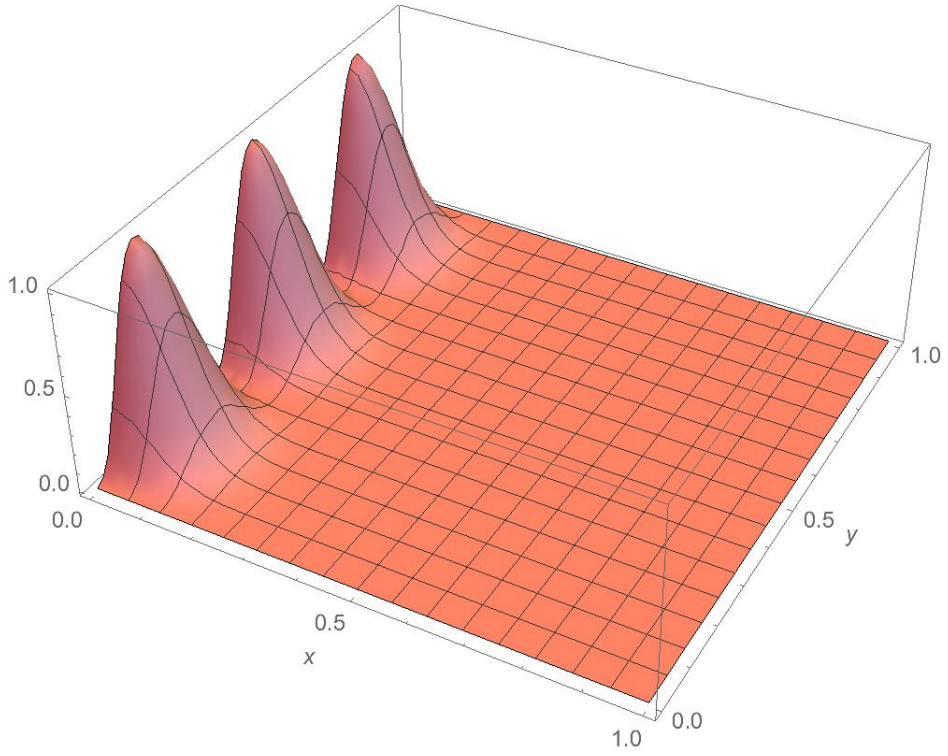

FIGURE 6.2: A plot of the initial distribution for cell density $n(x, y, 0)$ showing the three clusters emerging from the parent vessel. Generated using Mathematica.

Consider the case of a uniform row of tumour cells along the edge $x = 1$ and the edge of the parent vessel situated along $x = 0$. The first event of the tumour-induced angiogenesis in this system is the secretion of TAF by the row of tumour cells at $x = 1$ giving to good approximation an initial TAF concentration of

$$c(x, y, 0) = e^{-\frac{(1-x)^2}{\epsilon_1}}. \tag{6.12}$$

After the TAF reaches the parent vessel, the basement membrane degrades at certain points to allow for the migration of cells. For simplicity, we will assume that it degrades at three equally spaced points, causing three initial clusters of cells to form. A mathematical model for the initial formation of capillary buds is given in [9]. To represent the clusters, we use the initial condition

$$n(x, y, 0) = e^{-\frac{x^2}{\epsilon_3}} \sin^2(3\pi y) \tag{6.13}$$

which has been plotted in Figure 6.2.

The initial damage to the basement membrane results in an increased vessel permeability which allows fibronectin to leak from the parent vessel into the tissue. This results in a high initial concentration of fibronectin in and around the parent vessel. For this reason we take the initial fibronectin concentration to be

$$f(x, y, 0) = ke^{-\frac{x^2}{\epsilon_2}}. \tag{6.14}$$

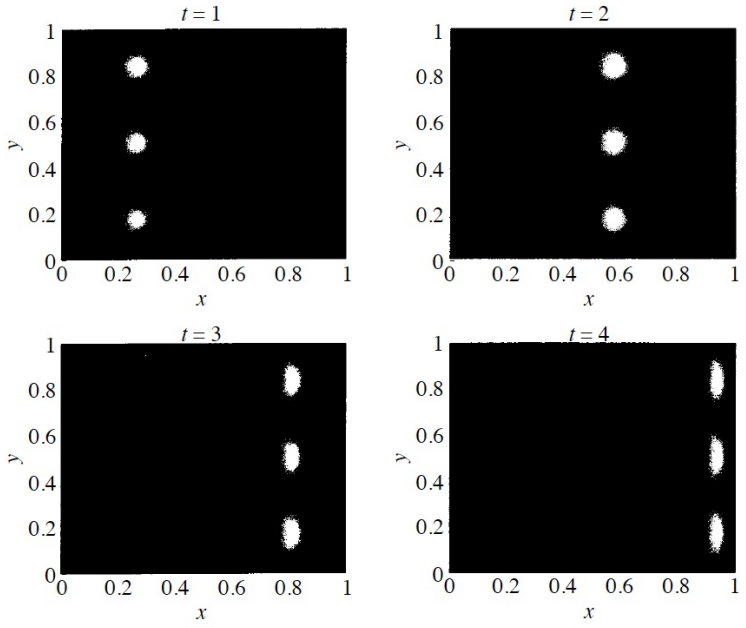

FIGURE 6.3: Spatiotemporal evolution of the endothelial cells for a system with no haptotaxis ($\rho = 0$). Lighter shading represents higher cell densities. Taken from [5].

With the equations and conditions in place, a finite difference approximation is used to generate numerical simulations of the model. The zero-flux conditions and absence of cell proliferation/death imply that the total cell number is conserved. We will vary the haptotactic coefficient ρ to determine the effects of haptotaxis on the angiogenic process.

For the case with no haptotaxis ($\rho = 0$), the simulation is given in Figure 6.3. Note there is very little lateral movement (displacement in the y-direction) and the system retains the form of the the initial distribution. The cell clusters have almost crossed the domain by $t = 4$ which is 6 days. (One unit of time is equivalent to 1.5 days.)

The second simulation, as shown in Figure 6.4, includes the effect of haptotaxis by increasing ρ but keeping all other parameters fixed. We see that haptotaxis has stimulated some lateral movement, causing the clusters to spread and merge with each other. Migration speed towards the tumour has greatly reduced and even by 15 days the cells have not reached a tumour, but formed a band with highest cell density at the leading edge. In fact, the band of cells never reaches the tumour. This is in agreement with [10], where it is demonstrated experimentally that although vascular sprouting can occur without cell proliferation, growth of the capillary network stops after a few days, failing vascularisation of the tumour. We will go on to include cell proliferation in the following chapter, where we consider a discrete model.

From this model we can conclude that the presence of fibronectin within the ECM allows for lateral movement via haptotaxis, causing cell clusters to merge and form a band. This however, slows down migration towards the tumour cells, and without the aid of cell proliferation the band never reaches the tumour. Note that we have not been able to fully incorporate the microscopic processes of sprout branching and anastomosis. Continuous models will often gloss over the finer details, so we move to

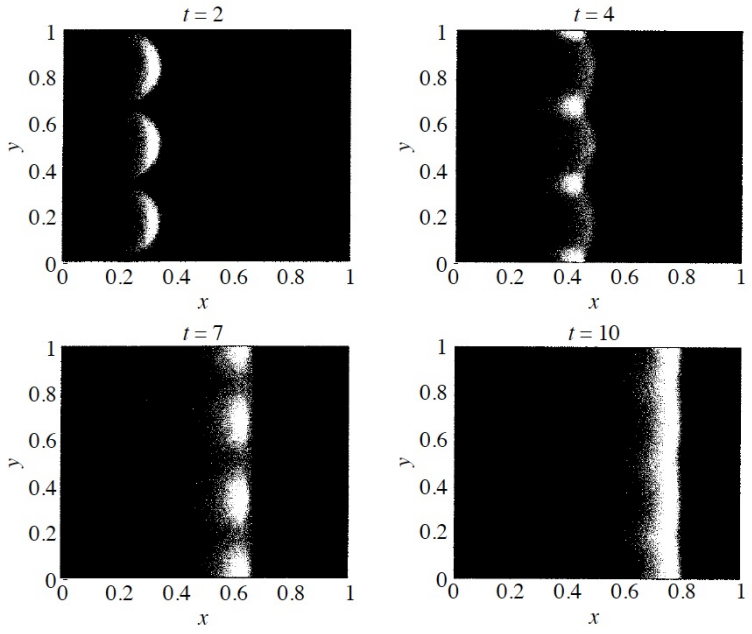

FIGURE 6.4: Spatiotemporal evolution of the endothelial cells with haptotaxis ($\rho \geq 0$). Lighter shading represents higher cell densities. Taken from [5].

looking at a discrete model that can follow the path of an individual cell at a sprout tip. In this way, we get a better insight into the structure of the capillary network produced.

Chapter 7

A Discrete Model

7.1 The advantages to discrete modelling

Until now we have only focussed on continuous deterministic models to simulate angiogenesis. This has produced some insightful results, however it lacks the incorporation of some of the finer details at the microscopic level. A discrete model allows us to follow the path of an individual cell at a sprout tip, so that when sprout paths are plotted, we can see the exact structure to the formed capillary bed. We can assign mathematical 'rules' to govern when branching and anastomosis can take place, and how this affects the system. Spatial movement is governed by nearest neighbour interactions based on a discretised form of the continuous model.

Using a discretised form of the equations also allows us to bring in stochasticity to the system, which is inherently present in angiogenesis.

7.2 Set-up of a Discrete Model

The particular model we review [5] discretises equations (6.9) to (6.11) and the domain $[0,1]\times[0,1]$ is split up into a grid of discrete points with mesh size h. Hence any point on the grid can be represented by integers (l,m) where the position of this point is then given by $x = lh, y = mh$. We discretise time into increments of magnitude k so $t = qk$. Notation is such that $n^q_{l,m}$ represents the number of cells at position $(x,y) = (lh, mh)$ and time $t = qk$ for some integer q.

The equation for the endothelial cells is then given by

$$n^{q+1}_{l,m} = n^q_{l,m}P_0 + n^q_{l+1,m}P_1 + n^q_{l-1,m}P_2 + n^q_{l,m+1}P_3 + n^q_{l,m-1}P_4 \tag{7.1}$$

where the coefficients $P_0 - P_4$ can be though of as being proportional to the probabilities of the endothelial cell being stationary (P_0), moving left (P_1), right (P_2), up (P_3) or down (P_4). Each time-step of the simulation process involves solving the discrete form of the system of equations (6.9) to (6.11) numerically to generate these coefficients.

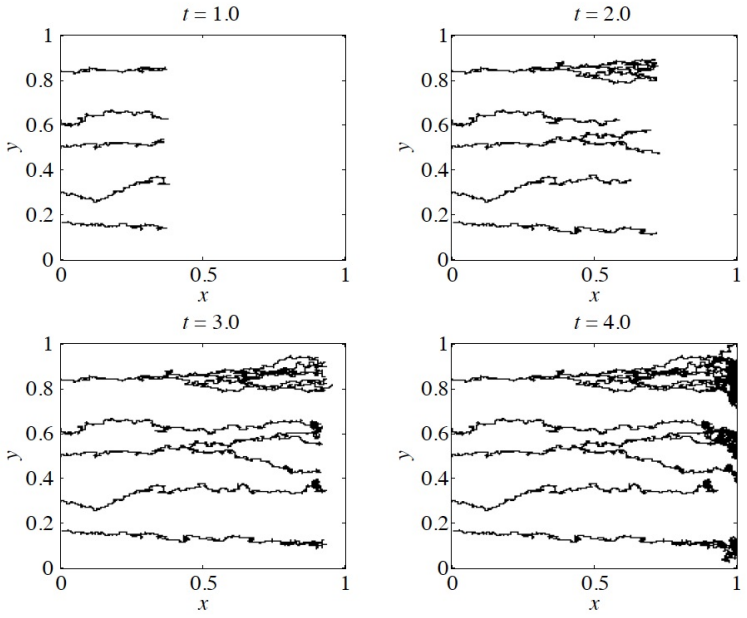

FIGURE 7.1: A numerical simulation that represents the spatiotemporal evolution of a capillary network migrating from the parent vessel ($x = 0$) to a row of tumour cells ($x = 1$) in absence of haptotaxis. Capillaries move almost directly towards the tumour cells with very little lateral movement. Taken from [5].

We now discuss the rules for branching and anastomosis and how they represent the corresponding biological characteristics. We make three requirements for branching to take place:

1. It is reasonable to assume that new sprouts do not branch immediately. We define a threshold branching age ψ, which the sprouts must exceed before they can branch.

2. There must be a sufficient number of cells in a sprout in order to branch. It has been observed that more branching occurs in the presence of higher densities of TAF. We therefore introduce a cell number threshold level n_b which is inversely proportional to the TAF density. As the cells come near to the tumour where there is a higher TAF density, sprout branching therefore increases dramatically. This is known as the 'brush border' effect.

3. Sprout branching requires sufficient space locally. If a grid position is already taken by another sprout, it cannot be used for branching.

Should all of these conditions hold at a certain position and time, there is a probability P_b that branching then takes place onto the next time step. P_b is taken to increase from 0 to 1 as the TAF concentration increases.

We assume anastomosis occurs when two sprout tips move to the same grid position. From this point on we then only consider one of the original sprout tips (chosen at random) holding the total number of cells.

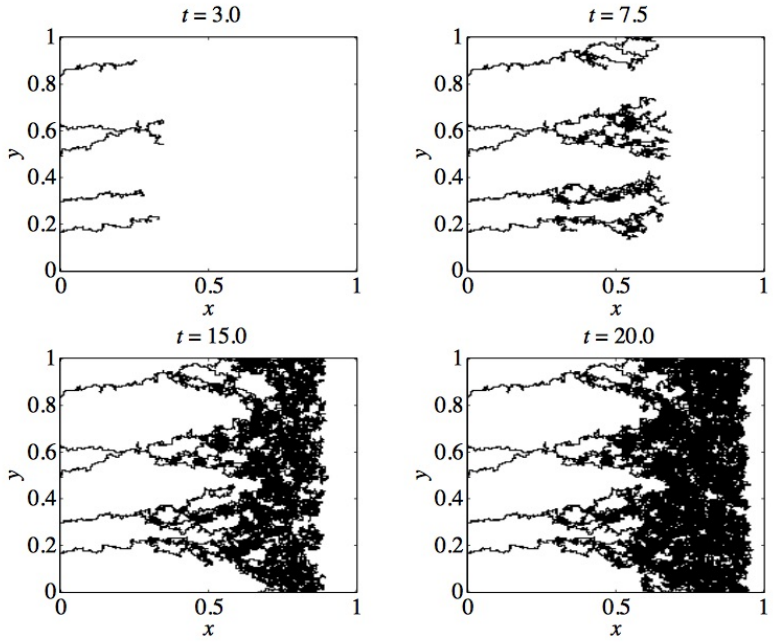

FIGURE 7.2: A numerical simulation that represents the spatiotemporal evolution of a capillary network migrating from the parent vessel ($x = 0$) to a row of tumour cells ($x = 1$) with the inclusion of haptotaxis. Lateral movement and anastomosis is observed, though slow progress towards the tumour cells. Taken from [5].

7.3 2D Simulations

In this section we consider simulations of the discrete model for three distinct cases. In the first case, haptotaxis is absent and the simulation is given in Figure 7.1. We then include haptotaxis which is demonstrated in Figure 7.2. Finally we incorporate cell proliferation into the model, shown in Figure 7.3.

7.3.1 No Haptotaxis

In agreement with the continuous model, the absence of haptotaxis results in very little lateral movement as can be seen in Figure 7.1. As a cause of this, no anastomosis has taken place, and very little sprout branching, so only a weak vascular structure has formed (this would be problem in wound healing). Note the randomness that is inherent in the model can be observed in that some sprouts are progressing faster than others. Contact is made with the tumour at an early time of $t = 4$.

7.3.2 Inclusion of Haptotaxis

With the inclusion of haptotaxis, we can see from Figure 7.2 that anastomosis occurs as early as $t = 3$. However overall migration towards the tumour is greatly slowed down. Observe the 'brush border' effect as the cells come near to the tumour in agreement with experimental observations.

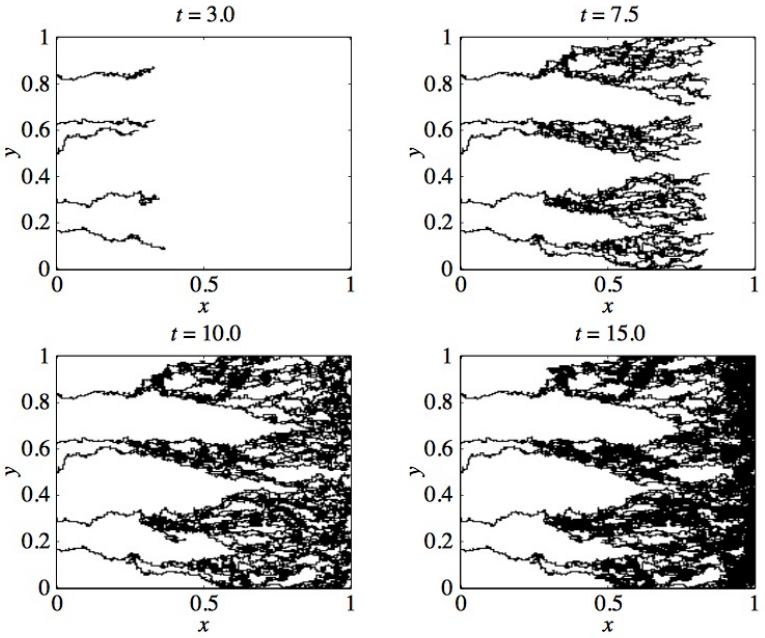

FIGURE 7.3: A numerical simulation that represents the spatiotemporal evolution of a capillary network migrating from the parent vessel ($x = 0$) to a row of tumour cells ($x = 1$) with the inclusion of haptotaxis and cell proliferation. Vascularisation of the tuour is achieved. Taken from [5].

Note that this simulation is consistent with the continuous case, so despite the previous model being deterministic, it still captures many of the important features of the process.

From the continuous and discrete simulations we can see the importance of cell-ECM interactions via haptotaxis in achieving both anastomosis and generation of sufficient vasculature. However the cells do not reach the target tumour in the case of haptotaxis; the absence of cell proliferation prevents the completion of angiogenesis.

7.3.3 Inclusion of cell proliferation

Experimental observations show that cell mitosis occurs about 48 hours into the process of angiogenesis. It is then the cells just behind the sprout tip that are most prolific. They divide approximately once every 18 hours, which contributes towards the sprout length. We include this process into our model by increasing each sprout length by an amount h (the approximate diameter of an endothelial cell) every half time unit (18 hours). The simulation is plotted in Figure 7.3.

The early stages are of course very similar to that in Figure 7.2 since cell proliferation does not start immediately. By $t = 7.5$ we see that with the aid of cell proliferation, a well-developed branching network has started to form. By $t = 10$, the sprouts have already come into contact with the tumour, in contrast with Figure 7.2 where the sprouts come to a halt at around $t = 20$.

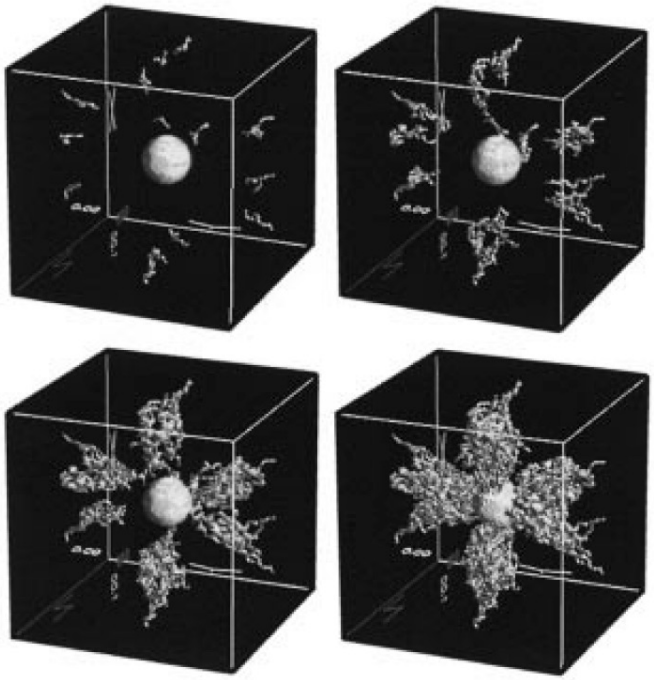

FIGURE 7.4: A three-dimensional simulation that represents the spatiotemporal evolution of a capillary network migrating towards a spherical source of tumour cells. Taken from [6].

7.4 A more realistic 3D simulation

While the results of the two-dimensional simulations are in excellent agreement with experimental results, tumour-induced angiogenesis occurs in a three dimensional microenvironment. The model can be extended [6] to include new probability coefficients P_5 and P_6 to correspond to movement up and down (perpendicular to the plane which we were working with previously). Once again, these coefficients are functions of the fibronectin and TAF concentrations near an individual endothelial cell.

We use a three dimensional grid this time, and generate the coefficients $P_0 - P_6$ from the discretised form of the dynamical equations (6.9) to (6.11). We shall consider the response of new capillaries to a spherical tumour source positioned at the centre of the tissue (modelled by a cube). The initial TAF concentration will therefore radially symmetric about the point $\vec{x_0} = (1/2, 1/2, 1/2)$, with a high concentration at the source decaying to lower concentrations at the boundaries.

It can be shown [11] that the initial TAF concentration can be given to a very good approximation by

$$c(\vec{x}, 0) = c(r) = \begin{cases} 1 & 0 \leq r \leq 0.1 \\ (1-r)^2/0.81 & r > 0.1 \end{cases} \tag{7.2}$$

where

$$r = \sqrt{(x-1/2)^2 + (y-1/2)^2 + (z-1/2)^2} \tag{7.3}$$

and the tumour cells are assumed to occupy the region $r \leq 0.1$.

The initial fibronectin concentration is assumed to be constant throughout the cube. Three initial sprouts are placed randomly placed on five out of the six faces giving 15 initial sprouts in total. Their progress is simulated and plotted at four different time steps a day apart in Figure 7.4.

We see that during the first two days, sprouts make their way towards the tumour, though little branching and anastomosis occurs. By day three, there are sufficient sprouts for some anastomosis to occur, which leads to a better connected vasculature. Recall that as the sprouts get closer to the tumour, sprout branching increases dramatically due to the increased TAF gradient. This is very notable from day three to day four where we can observe the three dimensional 'brush border' effect creating a dense vasculature which engulfs the tumour.

Chapter 8

Discussion

Angiogenesis is a complex process, involving many inter-connected variables. To formulate a single mathematical model that includes all of the relevant processes is a formidable task. Therefore, approaches have been taken to focus on specific aspects of angiogenesis separately. In spite of this, numerical simulations have agreed well with experimental data [12], and we have been able to extract interesting results from analysing the systems of equations.

The models reviewed here have incorporated several of the key mechanisms involved in the angiogenic process, however, extensions are of course still possible. One advance could be to investigate the structure of the formed capillary network. Experimental results have shown that disruption of certain receptors of the endothelial cells leads to a poorly formed capillary network, lacking in a full branching structure. Understanding the cause of these events and how to counteract them is vital in the promotion of successful wound healing.

One might consider modelling using additional angiogenic factors, depending on the circumstances. It is known that some factors induce a mitogenic response while others induce a migratory response. This is a useful approach in testing for optimal treatment mechanisms. Another modelling approach could include the blood flow through the capillary network, with potential application to drug delivery and optimisation of chemotherapy regimes. Indeed, there are many ways in which the mathematical frameworks constructed in this review can be adjusted and experimented with to aid medical understanding and the development of practical, clinical treatments on wounds.

Appendix A

Finer details for Chapter 3

A.1 Definitions for dimensionless parameters and motivation for parameter estimates

After having rescaled the system of equations developed in Chapter 3, we introduced new dimensionless parameters which are defined as follows:

$$\begin{aligned} C_1 = \frac{D_1 T}{L^2},\ C_2 = \frac{D_2 T b_0}{L^2},\ \ k_2 = \lambda_2 T,\ \ k_3 = \lambda_3 n_0 T, \\ k_4 = \lambda_4 b_0 T,\ \ k_5 = \frac{\lambda_5 n_0}{b_0}, \tilde{\chi} = \lambda_6 T b_1 n_0 \chi,\ \ \tilde{\nu} = \lambda_6 T b_0 \nu, \\ \beta = \frac{b_1}{b_0},\ \tilde{\zeta} = \frac{\zeta}{L},\ \ \tilde{n}_{init} = \frac{n_{init}}{n_0}. \end{aligned} \tag{A.1}$$

Upon analysing the stability of the steady states, we used the conditions that $k_2 = k_3$ and $k_4 > k_2$.

Recall the rescaling for the capillary tip density $\tilde{n} = \frac{n}{n_0}$. Without loss of generality, we may conveniently define n_0 to be the capillary tip carrying capacity. Looking back at the tip kinetics given by (3.2) we see the first two terms represent a logistic growth given by

$$f_{logistic} = \lambda_3 n(\frac{\lambda_2}{\lambda_3} - n) = \lambda_3 n(n_0 - n). \tag{A.2}$$

So with this definition of n_0 we have $n_0 = \frac{\lambda_2}{\lambda_3}$. Using (A.1) we see

$$\frac{k_2}{k_3} = \frac{\lambda_2}{\lambda_3 n_0} = 1 \tag{A.3}$$

and hence $k_2 = k_3$.

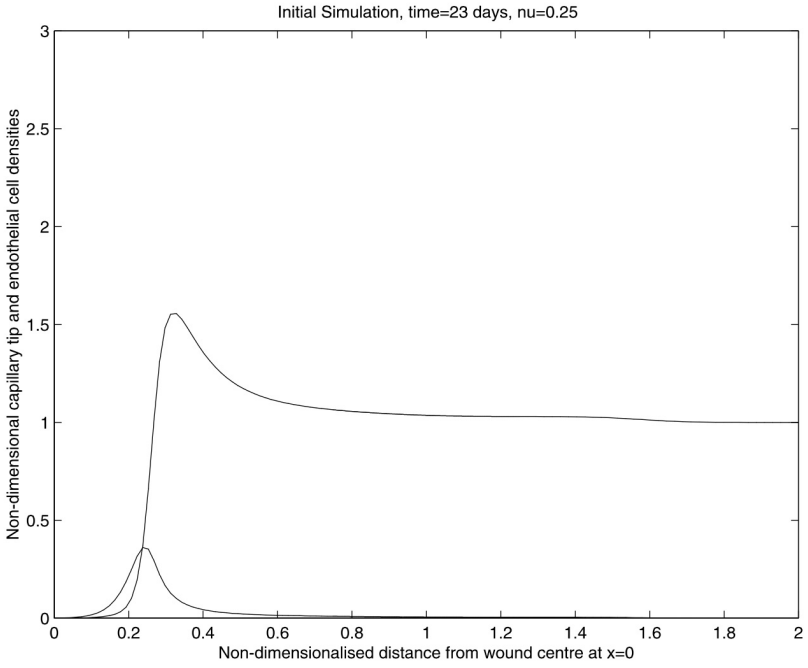

FIGURE A.1: A simulation at time 23 days with ν increased to 100 times its original parameter value. Travelling wave behaviour is exhibited. Taken from [2].

A.2 A Mathematical Curiosity

We found in section 3.2.4 that the characteristic lengthscale for the decay of the waveback of B exceeded the biologically relevant domain. At first sight, this appears to be a hindrance to our assumption of a travelling wave form for the angiogenic response. One might wonder how the simulation were to differ if we increase the cell proliferation rate ν and hence decrease l.

Figure A.1 shows the simulation at time 23 days, with the cell proliferation rate sped up by 100 times. Now $l \sim O(0.1)$, one tenth of the characteristic wound length, so the decay length is now within the biologically relevant domain. The resulting (n, b) profile exhibits a much steeper b tail and a travelling wave structure (to an excellent approximation) whereby it is simply translated with increasing time.

A.3 Speed of the Structural Unit

In Section 3.3.1 we hypothesised that the structural unit moves at the minimum travelling wave speed c_{min}. There are rigorous proofs for analogous hypotheses with scalar equations, though unfortunately this is lacking for cases like ours, involving a system of equations. However, numerical observations have all been consistent with our hypothesis in that the speed of the structural unit settles on the minimum travelling wave speed to close precision. Any discrepancies are small and arise since the travelling wave does not take into account the initial evolution of the wavefront. It has been shown that this discrepancy tends to zero on an extended biological domain.

Bibliography

[1] Graeme Pettet, Mark Chaplain, Sean McElwain, and Helen Byrne. On the role of angiogenesis in wound healing. *The Royal Society Publishing*, 1996.

[2] Eamonn Gaffney, K. Pugh, Philip Maini, and Frank Arnold. Investigating a simple model of cutaneous wound healing angiogenesis. *Journal of Mathematical Biology*, 2002.

[3] Luke Olsen, Jonathan Sherratt, Philip Maini, and Frank Arnold. A mathematical model for the capillary endothelial cell-extrcellular matrix interactions in wound healing angiogenesis. *IMA Journal of Mathematics Applied in Medicine and Biology*, 1997.

[4] Jonathan Sherratt and James Murray. Models of epidermal wound healing. *Proc. R. Soc, Lond.*, 1990.

[5] Alexander Anderson and Mark Chaplain. Continuous and discrete mathematical models of tumor-induced angiogenesis. *Bulletin of Mathematical Biology*, 1998.

[6] Mark Chaplain. Mathematical modelling of angiogenesis. *Journal of Neuro-Oncology*, 2000.

[7] James Murray. *Mathematical Biology.* Springer-Verlag, 1989.

[8] Knighton David, Ian Silver, and Thomas Hunt. Regulation of wound-healing angiogenesis-effect of oxygen gradients and inspired oxygen concentration. *Surgery*, 1981.

[9] Michelle Orme and Mark Chaplain. A mathematical model of the first steps of tumour-related angiogenesis: Capillary sprout formation and secondary branching. *IMA Journal of Mathematics Applied in Medicine and Biology*, 1996.

[10] M. Sholley, H. Ferguson, L. Seibel, J. Montour, and J. Wilson. Mechanisms of neovascularization. vascular sprouting can occur without proliferation of endothelial cells. *Laboratory Investigation: a Journal of Technical Methods and Pathology*, 1984.

[11] Mark Chaplain. The mathematical modelling of tumour angiogenesis and invasion. *Acta Biotheoretica*, 1995.

[12] H Byrne, M Chaplain, D Evans, and I Hopkinson. Mathematical modelling of angiogenesis in wound healing: Comparison of theory and experiment. *Journal of Theoretical Medicine*, 1999.